NATIONAL AERONAUTICS AND SPACE ADMINISTRATION

Technical Report 32-1569

Determination of Solid-Propellant Transient Regression Rates Using a Microwave Doppler Shift Technique

Leon D. Strand
August L. Schultz
Gary K. Reedy

JET PROPULSION LABORATORY
CALIFORNIA INSTITUTE OF TECHNOLOGY
PASADENA, CALIFORNIA

October 15, 1972

NATIONAL AERONAUTICS AND SPACE ADMINISTRATION

Technical Report 32-1569

Determination of Solid-Propellant Transient Regression Rates Using a Microwave Doppler Shift Technique

Leon D. Strand
August L. Schultz
Gary K. Reedy

JET PROPULSION LABORATORY
CALIFORNIA INSTITUTE OF TECHNOLOGY
PASADENA, CALIFORNIA

October 15, 1972

Preface

The work described in this report was performed by the Propulsion Division of the Jet Propulsion Laboratory.

Acknowledgment

The basic apparatus for this study was developed by the initial investigator, Dr. S. V. Shelton.

The following assistance is also gratefully acknowledged: Professor F. E. C. Culick and Mr. W. L. Dowler for helpful discussions and guidance, Dr. D. J. Norton for development of the solenoid triggering circuit and for quasi-steady-state regression rate measurements, Messrs. B. J. Barker and R. P. McNamara for assistance in carrying out tests, and Messrs. C. Feldstein, W. A. Trapp and R. E. Grafius for instrumentation support.

Contents

Tables

Contents (contd)

Figures

Contents (contd)

Abstract

A microwave Doppler shift system, with increased resolution over earlier microwave techniques, was developed for the purpose of measuring the regression rates of solid propellants during rapid pressure transients (10^4–10^5 N/cm^2-s). A continuous microwave beam is transmitted to the base of a burning propellant sample cast in a metal waveguide tube. A portion of the wave is reflected from the regressing propellant–flame zone interface. The phase angle difference between the incident and reflected signals and its time differential are continuously measured using a high resolution microwave network analyzer and related instrumentation. The apparent propellant regression rate is directly proportional to this latter differential measurement.

Experiments were conducted to verify the (1) spatial and time resolution of the system, (2) effect of propellant surface irregularities and compressibility on the measurements, and (3) accuracy of the system for quasi-steady-state regression rate measurements. The microwave system was also used in two different transient combustion experiments: in a rapid depressurization bomb, and in the high-frequency acoustic pressure environment of a T-burner. Polyether-polyurethane, hydroxy-terminated polybutadiene, and carboxyl-terminated polybutadiene/ammonium perchlorate composite propellants were tested.

In the rapid depressurization tests the measured apparent regression rates generally fell near or below the steady-state rate at the corresponding pressure and exhibited oscillations in tests near the critical depressurization rates for extinguishment. The results seem to reinforce the description of rapid depressurization extinction presented by Steinz and Selzer. Comparisons with the only other known transient data, that of Yin and Hermance, yielded both points of agreement and disagreement.

Unreasonably high oscillatory regression rates were obtained in the T-burner experiments. A set of parametric calculations were carried out, the results of which predict that flame ionization effects could be of sufficient magnitude to account for these high response results.

A direct comparison of the analytical predictions and experimental results yielded the conclusion that flame ionization effects probably produced some errors in the absolute values, but not the general characteristics, of the rapid depressurization regression rate measurements.

Determination of Solid-Propellant Transient Regression Rates Using a Microwave Doppler Shift Technique

I. Introduction

An area of solid-propellant rocket technology that has received a considerable amount of study is the burning of solid propellants under conditions of rapidly changing (i.e., transient) pressure. Two examples of such conditions are termination of rocket thrust by abruptly dropping the rocket chamber pressure (rapid depressurization extinguishment) and high-frequency acoustic combustion instability, which can involve pressure transients greater than 10^5 N/cm^2-s. The characteristic time of such pressure transients can approach, and be less than, the characteristic response time of the combustion process. Under such conditions propellant burning rates would be expected to deviate from steady-state predicted values. Theories devised to describe the above phenomena generally contain some type of expression, explicit or otherwise, for the nonsteady regression (Refs. 1–9). In the past, direct evaluation of such nonsteady-state combustion modeling has been hampered by the lack of comprehensive experimental data with which to compare theoretical results. The objective of this program was to develop a technique for providing such information.

The system finally arrived at yields an apparent regression rate by measuring the phase angle difference between an incident microwave signal propagating up a burning propellant test sample and the portion of the wave reflected from the regressing propellant–flame zone interface. Regression rate data were obtained under two highly transient pressure conditions: (1) during rapid depressurization in a combustion bomb, and (2) in the high-frequency oscillatory pressure environment of a T-burner. Data were taken for several propellant formulations containing ammonium perchlorate (AP) oxidizer with either polyether-polyurethane (PU), hydroxy-terminated polybutadiene (HTPB), or carboxyl-terminated polybutadiene (CTPB) binder systems.

In *Section II* of this report, some of the relevant transient combustion research performed by previous workers is discussed. *Sections III–VII* discuss details of the experimental technique, apparatus, test propellants, data acquisition system, and test procedure. In *Section VIII* the results are presented of tests conducted to verify the accuracy and resolution of the test system, and in *Section IX* the results of the transient regression rate measurements are presented. The apparent regression rates measured in the rapid depressurization experiments are compared with existing data. The unreasonably high oscillatory regression rates measured in the T-burner experiments led to the performance of a parametric analysis of the effects of rapid variations in the flame

zone ionization level on the microwave system transient regression rate measurements, the results of which are presented. The details of the calculation procedure are outlined in the *Appendix*. Finally, *Section X* attempts to summarize all of the experimental results that have been obtained and to draw conclusions as to the accuracy and limitations of the experimental technique.

II. Summary of Earlier Results

There have been a variety of methods, besides actual measurement of the regression rates, in which attempts have been made to experimentally observe the transient response of the combustion process to rapid perturbations in pressure. These have included dynamic pressure, optical, and spectral measurements of various types. Some of the pertinent results will be summarized to allow a comparison with the present findings.

Most experimental apparatus for transient combustion experiments include a high-frequency response transducer for transient pressure measurement. In attempts to provide a measure of the transient burning rate response through the behavior of the transient pressure, small-volume burners have been used, so that mass addition from the propellant surface during the transient period was appreciable in comparison to the mass initially contained in the chamber (characteristic time of the chamber small compared with that of the propellant). Wooldridge and Marxman (Ref. 7) used a powder pulse unit and nozzle plug to rapidly pressurize such a motor. Following the initial rapid pressure rise, the pressure rose to the final steady-state value in an oscillatory manner. In rapid depressurization experiments, Steinz and Selzer (Ref. 10) observed the presence of pressure oscillations in the 100-Hz frequency range at depressurization rates near the extinction boundary. They attributed them to irregularities in the flame.

Attempts have been made to deduce the gas evolution rates during depressurization from the measured pressure–time history (Refs. 11 and 12). Besides the difficulty just discussed of the characteristic time of the chamber being large enough to mask the transient effects, questions as to the assumed pressure dependency of the gas temperature (isothermal, adiabatic–isentropic, etc.?) and unsteadiness of the flow in the chamber (Ref. 13) make transient data obtained in this manner highly suspect.

Photo cells have been used to measure the total luminosity of the transient flame during depressurization since Ciepluch's original experiments (Ref. 14). More recently, flame temperature measurements have been made using a spectrometer (Ref. 15) and thermocouples (Ref. 16). The results were quite similar. Typically, there was a millisecond or less delay in temperature response to the depressurization, followed by an abrupt decay, the magnitude of such depending on the severity of the depressurization. Except at the highest depressurization rates, the temperature would partially recover before decaying to ambient. Experiments measuring the luminous flux beneath the propellant surface also exhibited a lag behind the pressure decay (Ref. 12).

The flame during rapid depressurization has also been observed by high-speed photography (Refs. 10 and 17). In the experiments of Steinz and Selzer, the flame intensity fell to zero within the first millisecond. For initial depressurization rates $(dP/dt)_0$, less than 16×10^4 N/cm^2-s a second, sometimes irregular, flame developed after about 5 ms. This secondary flame did not extinguish until very near the end of the pressure transient, when the pressure had just about equalized with the back pressure.

Steinz and Selzer also measured spectrographically the intensities of the OH, NH, CN, and Na lines in the gaseous flame during depressurization. They found the intensity of the CN line to respond much faster to pressure perturbations than the Na line. This was attributed to adiabatic expansion quenching the active gaseous reactions, which in turn caused the temperature to drop still faster to below the luminosity threshold.

Baer, Ryan, and Schultz (Ref. 15) used a rapid-scanning spectrometer to obtain infrared emission spectra of propellant flames during depressurization. From measurements of H_2O and CO_2 bands, they concluded that during the initial rapid pressure drop the ammonium perchlorate gasification rate was increased relative to the fuel–binder decomposition. Later in the transient, a more fuel-rich period occurred.

The preceding studies have been concerned with the propellant combustion response to a single pressure perturbation. The response of a burning surface to oscillatory or harmonic pressure waves is commonly characterized by the response function, the dimensionless ratio of the mass flux perturbation normal to the propellant surface to the pressure perturbation. Considerable experimental investigation has been devoted to determining its magnitude and phase and how it varies with pressure, frequency, and propellant composition (Refs. 5 and 18). The experimental response function is generally calculated from the measured rate of growth and

decay of pressure oscillations in special burners of simple geometry (L^*-, T-burner).

Krier, et al., attempted to measure the gas temperature near the propellant surface in a large T-burner using an optical method (Ref. 19). In experiments at low frequencies (15–80 Hz), temperature and entropy waves were found at the same frequency as the pressure oscillations. The largest part of the entropy oscillation was attributed to be due to the thermal lag of the solid phase.

The spectrometer of Ref. 15 has also been used to study flame spectra during L^*-bulk mode instability at frequencies from 10 to 110 Hz (Ref. 20). Of special interest to the present study was their finding that the fluctuations in composition led the pressure by a phase angle of 0.25 to 0.88 radians (14 to 50 deg).

In summary, the transient response of the solid-propellant combustion process to rapid variations in pressure has been shown to be highly complex, featuring lags in response, oscillatory or irregular burning, and, for sufficiently high depressurization gradients, partial or complete extinguishment. As will be shown in *Section IX*, the transient regression rate data obtained in the present study generally agree with these observations.

III. Experimental Technique

To obtain regression rate data under transient pressure conditions, a technique with extremely accurate propellant-length resolution is required. For example, consider a propellant burning at a rate of 0.75 cm/s. If a depressurization occurs over a time interval of 15 ms, an average propellant displacement of 110 μm can be expected. To obtain reasonable definition of the regression rate curve, a minimum of 10 points would be desirable. This requires resolution of 10 μm or better. Obviously, mechanical, thermocouple, or optical scanning of the flame location is not satisfactory, especially considering that the oxidizer crystals may be of the order of 100 μm. The only previous technique claiming the required resolution is a variable capacitance system (Ref. 21), which will be discussed in detail in *Section IX-A-4*.

For the past several years a program was effected to develop and test a transient burning rate measurement system by substantially improving the resolution of earlier microwave techniques (Refs. 22–24, for example). Because of their low resolution, these earlier burning rate measurement techniques were suitable for use only in quasi-steady situations. A microwave system was first used for transient regression rate measurements by S. V. Shelton at the Jet Propulsion Laboratory (Ref. 25) following the introduction of a high-resolution, fast-response microwave network analyzer. The work presented here was done using Shelton's basic apparatus.

The principle of previous microwave techniques is illustrated in Fig. 1. A continuous microwave beam of frequency ω_i is transmitted to the base of a burning propellant sample. Reflections are generated at both the base of the sample and the burning surface. The base reflection remains at the incident frequency, ω_i, but the frequency of the burning surface reflection is Doppler-shifted by an amount $2k_p r$, where k_p is the microwave propagation constant in the propellant, and r is the surface regression rate. This result is obtained by applying two successive Galilean transformations to a plane wave. The superposition of these two reflected signals produces a beat frequency, $\Delta\omega = \omega_r - \omega_i$, which is measured by the detector (see Fig. 1), and from which the regression rate is calculated using the Doppler shift expression:

$$\Delta\omega = 2k_p r \tag{1}$$

This method is incapable of resolving rapid regression rate changes during pressure transients due to the long time required to determine the beat frequency ($T_{\text{beat}} = 2\pi/\Delta\omega \approx 1$ second).

The present microwave technique achieves greater resolution by monitoring the phase angle difference between the incident and reflected signals. The phase angle principle is illustrated in Fig. 2. The reference and test channels in Fig. 2, which monitor the incident and reflected signals, respectively, are the two input channels of a microwave network analyzer, which continuously measures the phase difference between the two signals. This phase difference can be separated into two parts: (1) path length phase difference (Doppler shift), and (2) burning surface phase shift. The difference in path length between the two measurement points produces a phase difference proportional to the path length. The constant of proportionality is known as the propagation or phase constant and depends on the geometry of the waveguide and the dielectric constant of the medium filling the waveguide. Here, in Fig. 2, we have two separate phase constants: k_w for the empty rectangular waveguide leading to the propellant sample, and k_p for the propellant sample tube. From Fig. 2, this part of the phase difference is given by

$$\phi_{\text{path length}} = k_w(b + c) + k_p(2\ell) \tag{2}$$

The second component of the phase difference, the burning surface phase shift ϕ_s, is caused by the jump in wave impedance at the burning surface. Its magnitude is dependent on conditions at the propellant–flame interface. It will be assumed to be constant for now, and will be discussed in greater detail in *Section IX-C* and in the *Appendix*. The total phase difference is thus given by

$$\phi_{\text{total}} = k_w(b + c) + k_p(2\ell) + \phi_s \tag{3}$$

Differentiating with respect to time and noting that $d\ell/dt = -r$, we finally obtain:

$$\frac{d\phi}{dt} = -2k_p r \tag{4}$$

The phase constant, k_p, is calculated from the same phase versus time record used in the regression rate calculation. The total propellant length burned, ℓ_0, and the total phase shift, ϕ_0, for an entire test are substituted into the integrated form of Eq. (4) to yield:

$$k_p = \frac{\phi_0}{2\ell_0} \tag{5}$$

Combining Eqs. (4) and (5), we obtain the final expression for the regression rate as a function of $d\phi/dt$:

$$r = \frac{\ell_0}{\phi_0}\left(\frac{d\phi}{dt}\right) \tag{6}$$

The wavelength of the microwave signal in the test propellant can also be calculated from the phase versus time record:

$$\lambda_p = \frac{\ell_0}{\phi_0/720°} \tag{7}$$

Substituting Eq. (7) into Eq. (6) yields another form of the regression rate equation:

$$r = \frac{\lambda_p}{720°}\left(\frac{d\phi}{dt}\right) \tag{8}$$

Inserting the measured value for λ_p, it can be shown from Eq. (5) that for a spatial resolution of 10 μm, a phase angle resolution of approximately 0.5 deg is required.

In actual practice the reflected signal into the network analyzer contains a small component oscillating at the source frequency, ω_i, due to reflections from impedance mismatches within the microwave system, which superimposes an oscillation of frequency $2k_p r$ on the phase angle signal. This has little effect on the transient measurements, since the time scale of the transient events is usually much smaller than the period of the superposed oscillation, but for burning rate measurements during gradual pressure changes, this oscillation must be taken into account in reducing the data. A more detailed description of this effect is given in Ref. 25.

IV. Apparatus

A block diagram of the microwave system is presented in Fig. 3. The radio frequency source is a reflex klystron operating near 10 GHz and stabilized by an oscillator synchronizer to $1/10^8$ Hz. The power level was 0.3 mW. The basic microwave transmission system is a standard rectangular X-band waveguide with coaxial cable leads to the instrumentation and a short section of circular waveguide near the combustion bomb. Immediately following the klystron is a 20-dB directional coupler which diverts 1% of the klystron output to the oscillator synchronizer for frequency stabilization and to a thermistor for power measurement. A ferrite isolator, which allows signal propagation in the forward direction only, is inserted to minimize the effect of reflected signals on the RF source. The second directional coupler diverts another 1% of the power to the reference channel of the microwave network analyzer for comparison with the signal reflected from the propellant sample. The remaining signal then passes through the E–H tuner, a reversed 10-dB directional coupler and the slide tuner to the propellant burning surface. The directional couplers are designed to couple only radiation propagating in a specified direction into the external circuit, thus minimizing the problem of mixing incident and reflected signals in the channels of the network analyzer. Signal mixing, or cross-talk, is further reduced by the E–H tuner placed between the couplers to the network analyzer. The slide tuner before the propellant sample is used to tune out the reflection from the base of the propellant sample. The signal reflected from the burning surface propagates back through the waveguide system to the reversed 10-dB directional coupler, which diverts 10% of the reflected signal to the test channel of the network analyzer, which produces dc voltages proportional to the phase and amplitude differences of the reference and test channel signals.

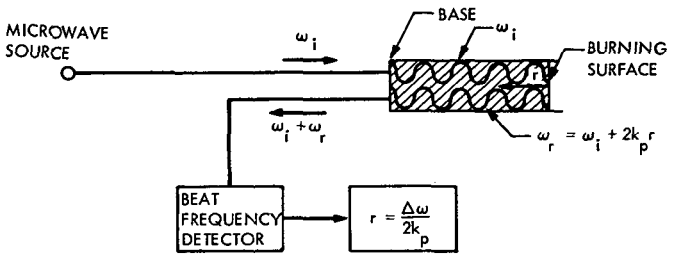

Fig. 1. Doppler shift principle

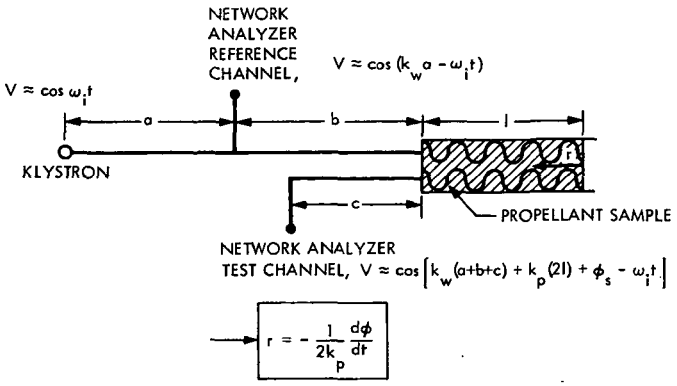

Fig. 2. Phase shift principle

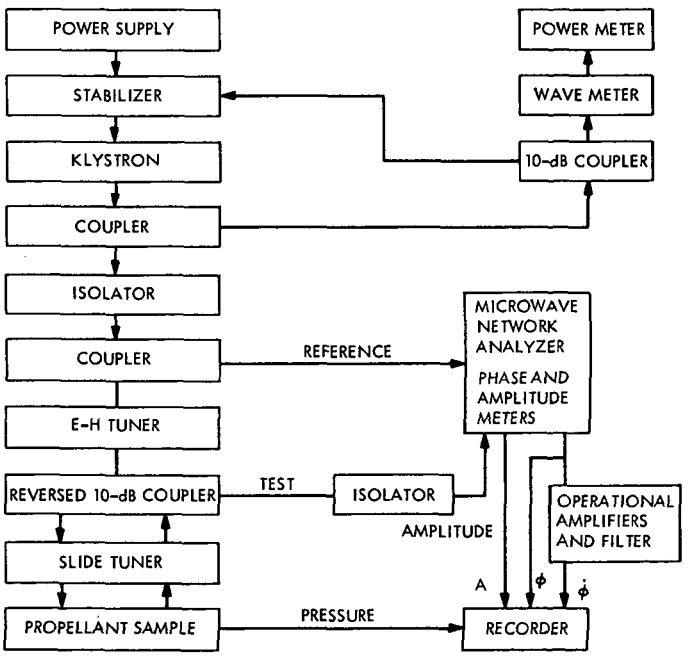

Fig. 3. Microwave system block diagram

The instrument panel is shown in Fig. 4. The phase and amplitude relationships of the reflected and reference waves were initially determined by means of three Hewlett-Packard instruments: the Model 8411A Frequency Converter, the Model 8410A Network Analyzer, and the Model 8413A Phase-Gain Indicator. The frequency converter and network analyzer, together, comprise a two-channel microwave receiver, and the phase-gain indicator detects the phase and amplitude relationships of one channel with respect to the other. The three instruments, in combination, contain five major sections: first converter, automatic gain control, second converter, phase and amplitude offset, and phase and gain determination (Figs. 5 and 6).

The first converter stage down-converts the signals on the two channels from their microwave frequency, approximately 10 GHz, to the first intermediate frequency of 20.278 MHz. The first converters utilize a technique known as "harmonic sampling" because it permits a single instrument to operate over an extremely broad range of input frequency, in this case from 110 MHz to 12.4 GHz.

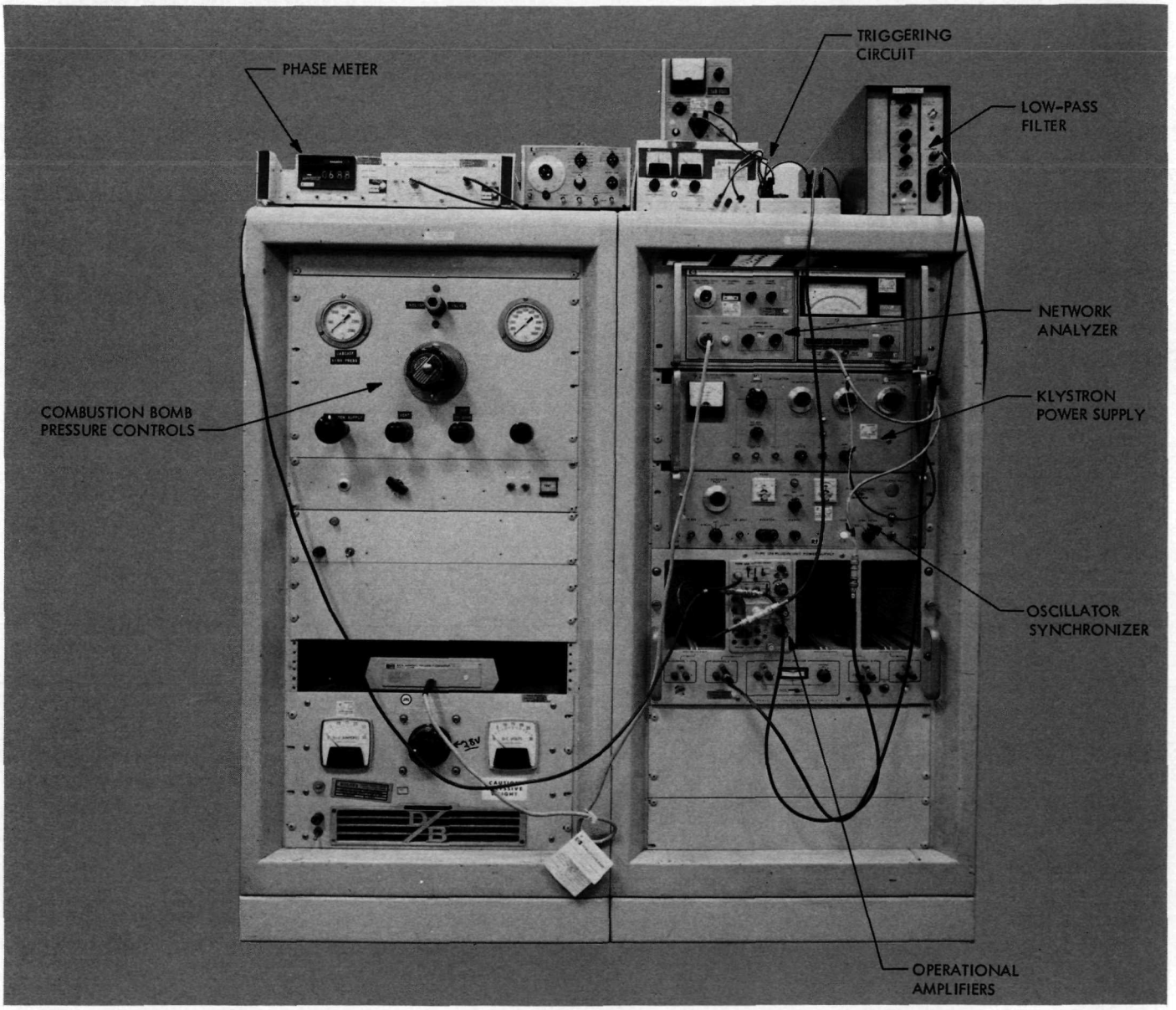

Fig. 4. Microwave control and instrument panel

Sampling is a process in which a high-frequency, repetitive signal is duplicated at a much lower frequency. The low-frequency signal is obtained by accumulating amplitude samples taken from different occurrences of, and at progressively later points on, the high-frequency waveform. The time taken to collect enough samples to reconstruct a cycle of the high-frequency signal is much longer than the period of one cycle of the sampled waveform. Thus, the high-frequency waveform is time-stretched to a low-frequency waveform. With appropriate timing of the samples, a faithful replica of the original signal is produced and subsequent operations can be done with low-frequency circuitry. The frequency of the local oscillator which drives the sampling circuitry is controlled by means of a phase-lock loop to automatically track variations of the incoming frequency, producing a constant first intermediate frequency of 20.278 MHz. The two samplers, one in each input channel, are driven by the same local oscillator, so that samples are taken at the same instant in each channel and the phase relationship of the two signals is not altered.

An automatic gain control section enables the network analyzer to make continuous, broadband measurements despite amplitude variations as great as 20 dB that are common to both microwave input signals. The automatic gain control loop holds the output level of the reference channel first intermediate frequency amplifier constant. The same gain-controlling signal that is applied to the reference channel amplifier is also applied to the first intermediate frequency amplifier of the other channel. Since these amplifiers are electrically matched, their gain variations track and the amplitude ratio display is unaffected by common mode variations in the amplitude of the microwave input signals. With the amplitude signal at the output of the reference channel held constant, the ratio of the test channel amplitude to the reference channel amplitude can be measured directly at the output of the test channel.

The second converter section employs a conventional crystal-controlled beat-frequency oscillator to produce a second intermediate frequency of 278 kHz. The mixers

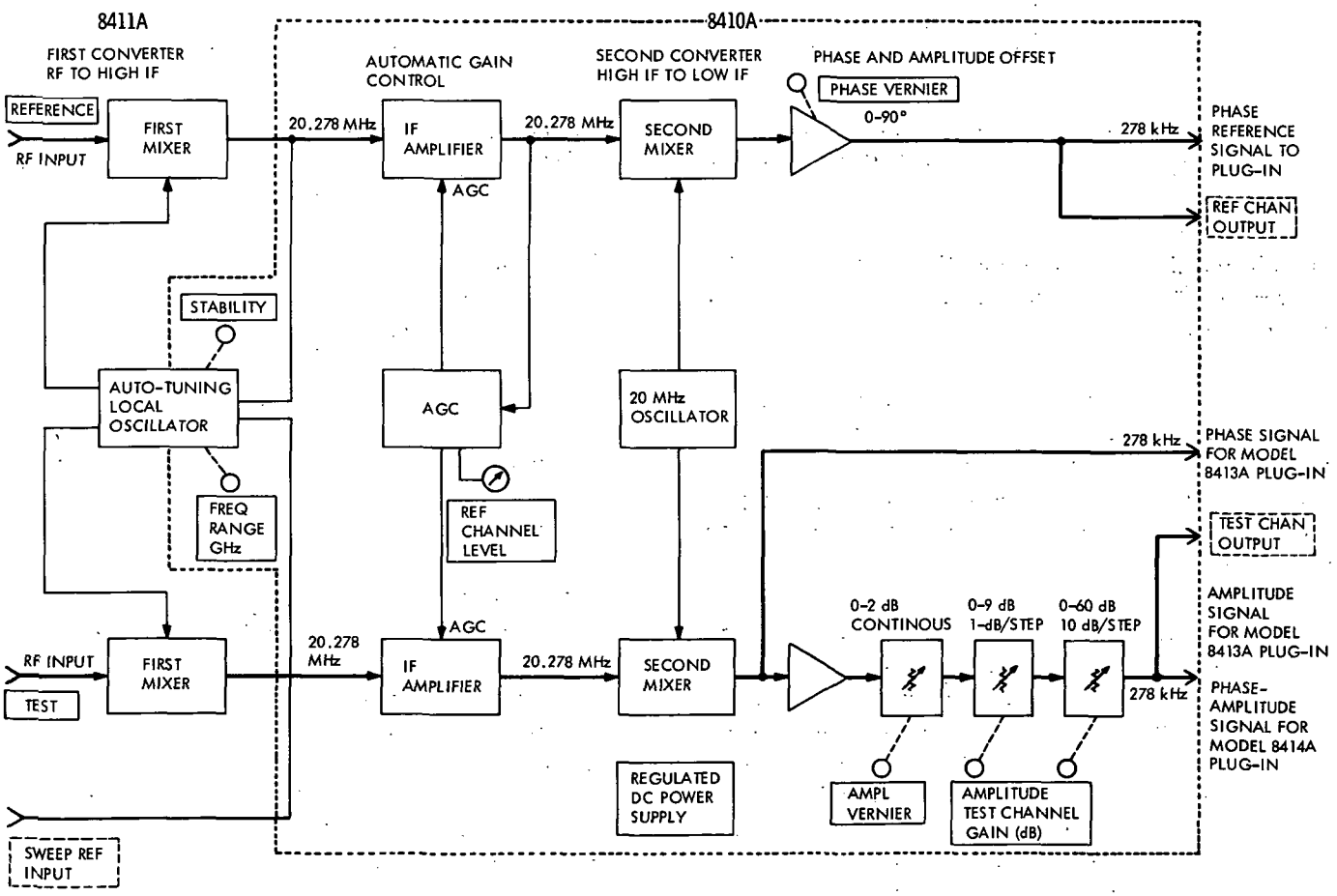

Fig. 5. Hewlett-Packard Model 8410/8411A basic block diagram (reprinted by permission of Hewlett-Packard Company)

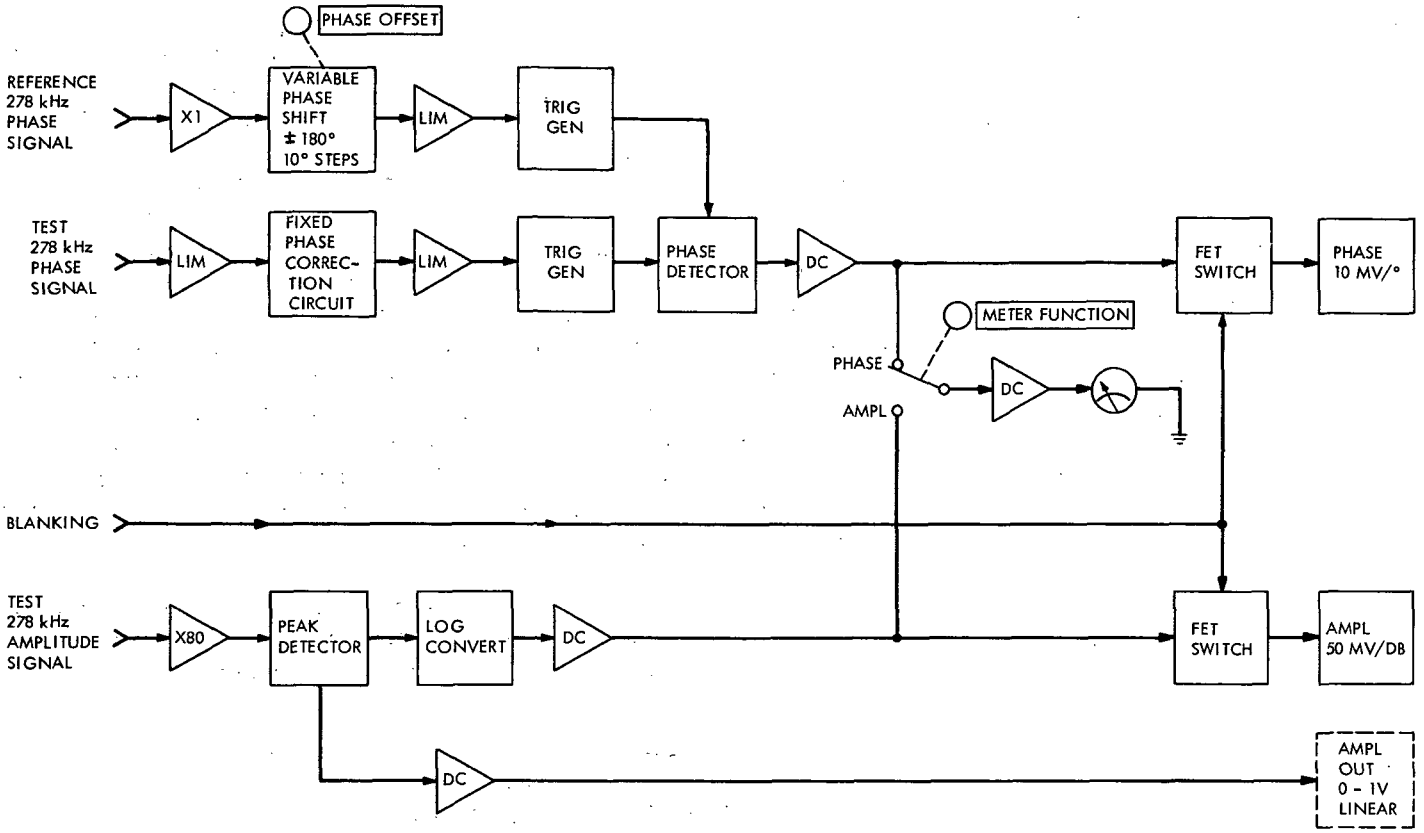

Fig. 6. Hewlett-Packard Model 8410/8411A Phase-Gain Indicator simplified block diagram (reprinted by permission of Hewlett-Packard Company)

of both channels are driven from the same local oscillator to preserve the relative phase relationship between their respective signals.

Calibrated phase and amplitude offset controls allow adjustment of the phase and amplitude relationships, if necessary, in order to permit use of the instrument at its maximum resolution over the complete range of phase difference from 0 to 360 deg and of amplitude ratio from 0 to 60 dB.

Finally, in the phase-gain indicator, the phase difference between the reference and test signals is determined by means of a phase detector circuit (Fig. 6). The reference and test signals each feed a Schmitt trigger multivibrator circuit. The outputs of the Schmitt triggers are fed to the phase detector multivibrator where the two signals are resolved into a dc signal which represents their phase difference. The scale factor of the phase difference signal is 10 mV/deg. Its minimum accuracy is ± 1.5 deg.

The amplitude ratio between the reference and test signals is determined by means of a peak-detector circuit. The detected peak signal is fed to a logarithmic converter whose dc output signal has the scale factor of 50 mV/dB. The accuracy of the amplitude ratio is $\pm 3\%$.

The phase signal output of the phase-gain indicator generally had imposed upon it random electronic noise over a wide frequency range, 0 to 10 kHz and greater. Even with selective low-pass filtering, the noise level (>1 deg) was greater than the desired phase angle resolution, prohibiting any time differential resolution.

Eventually a Dranetz Engineering Laboratories, Inc., Model 305 High Accuracy Phase Meter was incorporated to measure the phase difference between the reference and test signal outputs of the wave analyzer. Its dc signal output, also 10 mV/deg, is remarkably free of high-frequency noise, containing only the 278-kHz carrier frequency of the wave analyzer. It is capable of resolving a phase difference of ± 0.25 deg up to a frequency of

500 kHz, allowing a propellant surface spatial resolution of 5.4 μm.

With this clean phase signal, differentiation and amplification, employing two Type 3A8 Tektronix operational amplifiers (Fig. 7), permitted the propellant transient regression rate to be measured directly. From Eq. (8) the amplifiers were calibrated prior to each test using triangular wave signals from a Hewlett-Packard Model 3310 Function Generator. The output of the differential amplifier was determined to be linear up to a frequency of 100 Hz (Fig. 8). Above 100 Hz the output began departing from linearity, dropping off by 40% at 1000 Hz.

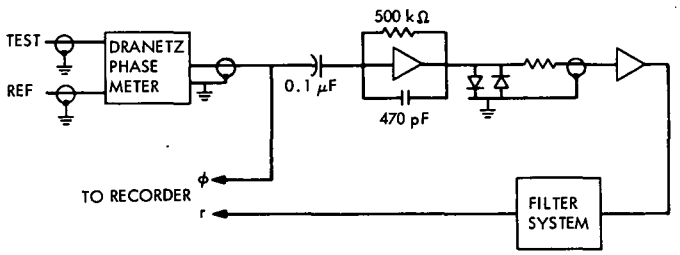

Fig. 7. Operational amplifier block diagram

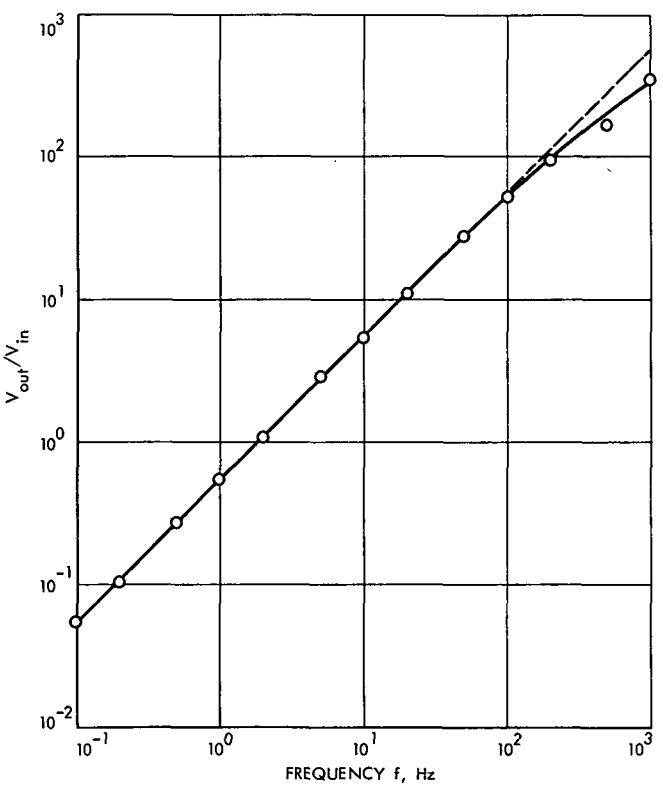

Fig. 8. Voltage-out/voltage-in ratio versus frequency for differential amplifier

Its phase shift was also found to be a function of frequency (Fig. 9), dropping to zero with increasing frequency. Where required, the experimental results were corrected to account for these nonlinearities in the test system.

The main difficulty in this differentiation operation is the generation of large-amplitude signals from low-amplitude noise impressed upon the phase signal at some point(s) in the circuit. The spurious noise on the differentiated signal (60 Hz, 300 Hz, and higher harmonics) was reduced to an acceptable level without destroying valid lower-frequency data or the necessary frequency response by using a 60-Hz narrow-band notch filter and selective low-pass filtering with a sharp cutoff filter (Dynamics 6371).

The microwave path through the propellant is shown in Fig. 10. The propellant samples are cast in 1.59-cm (⅝-in.) inner-diameter, 5.1-cm (2-in.) or 10.2-cm (4-in.) long steel tubes, threaded at each end, which serve as waveguides for the microwave. A large part of the fixed

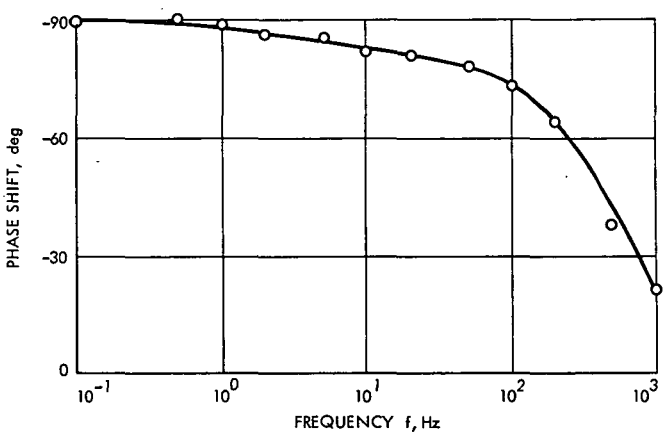

Fig. 9. Phase shift of differential amplifier versus frequency

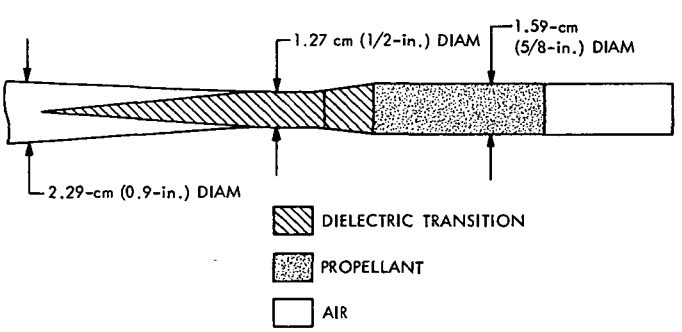

Fig. 10. Microwave electrical path

reflection in the microwave system originates at the propellant lower interface, since at this point the microwave signal must make a transition from air-filled rectangular waveguide to the propellant sample, which is effectively a dielectric-filled circular waveguide. To minimize the discontinuity at this transition, a long cone of Melmac plastic with dielectric properties similar to those of the propellant is inserted before the propellant sample. In addition to reducing the reflection from the air–propellant interface, the cone serves as a pressure sealing "window" for the test base plate.

The inside diameter of the propellant tube was sized to propagate with low losses only the microwave dominant mode when filled with propellant and to be below cutoff for all frequency modes when empty.

Solid-propellant regression rate measurements were conducted under two transient conditions: during rapid depressurization in a combustion bomb, and while exposed to acoustic oscillations in a T-burner.

Figure 11 shows some details of the 5.1-cm (2-in.) inner diameter by 15.24-cm (6-in.) long combustion bomb, with the propellant sample screwed into place. The assembled system prior to test is shown in Fig. 12. Bomb pressure was controlled by a regulated nitrogen supply and vent system and measured by a Taber strain gage transducer and a water-cooled Kistler Model 603A piezoelectric pressure transducer/Model 504 charge amplifier. Rapid depressurization on command was achieved by simultaneously closing a nitrogen supply solenoid valve and bursting the diaphragm with a solenoid-controlled knife blade. Various rates of depressurization were obtained by changing the orifice size. Venting in all tests was to atmospheric pressure.

A triggering circuit, shown schematically in Fig. 13, was used to synchronize the bursting of the diaphragm to the vicinity of $\phi = 0$, where the correction to the phase angle for fixed reflections was usually near zero. After being manually armed, the triggering circuit automatically activated at the next desired value of ϕ.

A cross-sectional diagram of the 6.35-cm (2.5-in.) diameter T-burner is shown in Fig. 14 and the complete test assembly in Fig. 15. Except for the adaptor for mounting the T-burner on the microwave base plate, all components were developed in a research program conducted earlier at JPL and are described in more detail in Ref. 26. Another modification was a 2.54-cm (1-in.) hole in the center of the lower disc of the acoustic driver propellant to permit the test propellant tube to pass through. A 5.1-cm (2-in.) long extension tube is shown attached to the propellant tube in Fig. 14. This was a later modification to the test system, and will be discussed in the section on T-burner test results. To obtain reasonable definition of the transient regression rate with a microwave system spatial resolution of 5 μm, a calculation similar to that presented in *Section III* gives an upper limit frequency of about 150 Hz. In these tests a T-burner length of 51 cm (20 in.) was used, giving a fundamental frequency of approximately 800 Hz. This higher than desirable frequency was dictated by the necessity to be in the region of maximum acoustic response for the A-13 driver propellant. The amplitude of pressure oscillations for this propellant was found to drop off sharply with decreasing frequency (Ref. 26).

The pressure in the T-burner was controlled by venting into a 0.2-m^3 (7-ft^3) surge tank (Fig. 15). Pressure instrumentation consisted of a Taber transducer for mean pressure measurement and a Kistler 603A for measuring the dynamic pressure. To compensate for thermal drifting, the latter signal was passed through coupling transformers having a flat frequency response between 0.05 and 15.0 kHz.

V. Propellants

The four propellants used in this study are listed in Table 1, along with general details of their composition. The 540A propellant has a near-stoichiometric composition and burns very clean. The other three propellants are under-oxidized and burn quite smokey. Steady-state

Table 1. Test propellant compositions

Propellant	Binder/ oxidizer	Binder/ oxidizer concentration, %	Oxidizer mass median diameter, μm
540A	PU[a]/AP[b]	20/80	17 (30%) 170 (70%)
HTPB[c]	HTPB/AP	17/83	17 (30%) 170 (70%)
CTPB[d]	CTPB/AP	25/75	17 (33%) 90 (67%)
CTPB-mod	CTPB/AP	25/73 (2% Al)	17 (33%) 90 (67%)

[a]Polyether-polyurethane.
[b]Ammonium perchlorate.
[c]Hydroxy-terminated polybutadiene.
[d]Carboxyl-terminated polybutadiene.

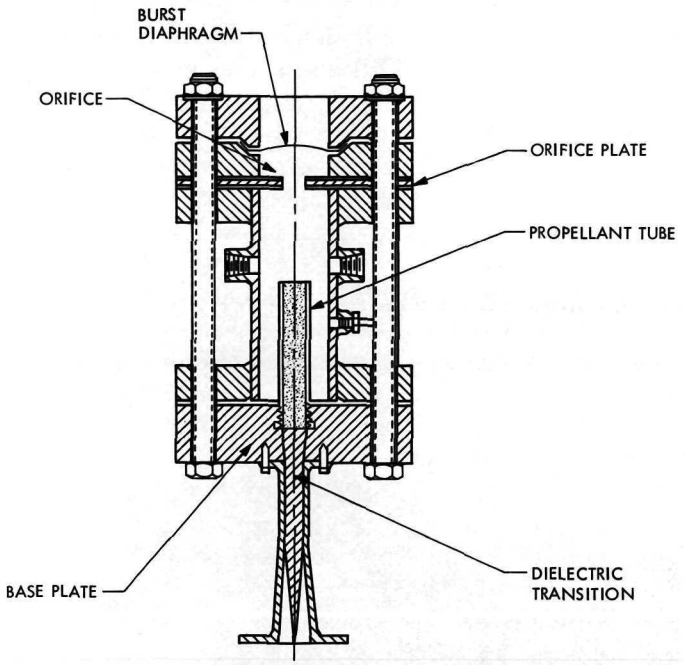

Fig. 11. Combustion bomb cutaway drawing

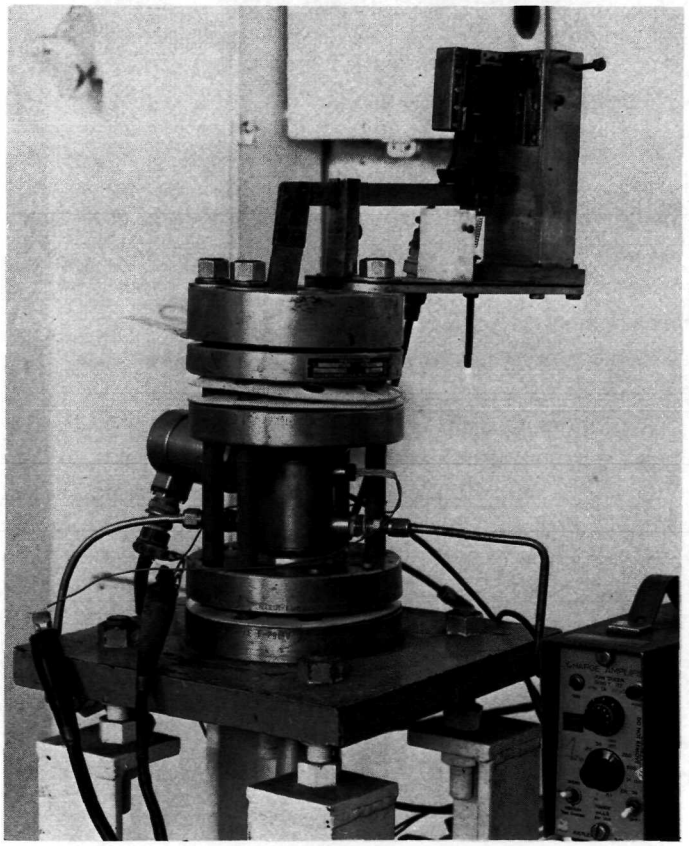

Fig. 12. Combustion bomb assembled for rapid depressurization test

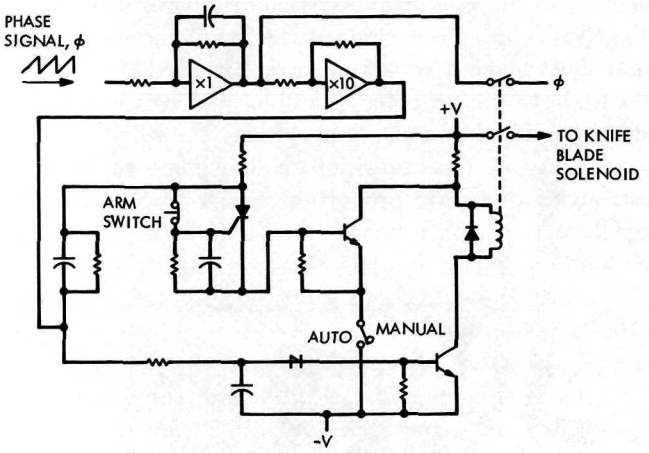

Fig. 13. Depressurization triggering circuit

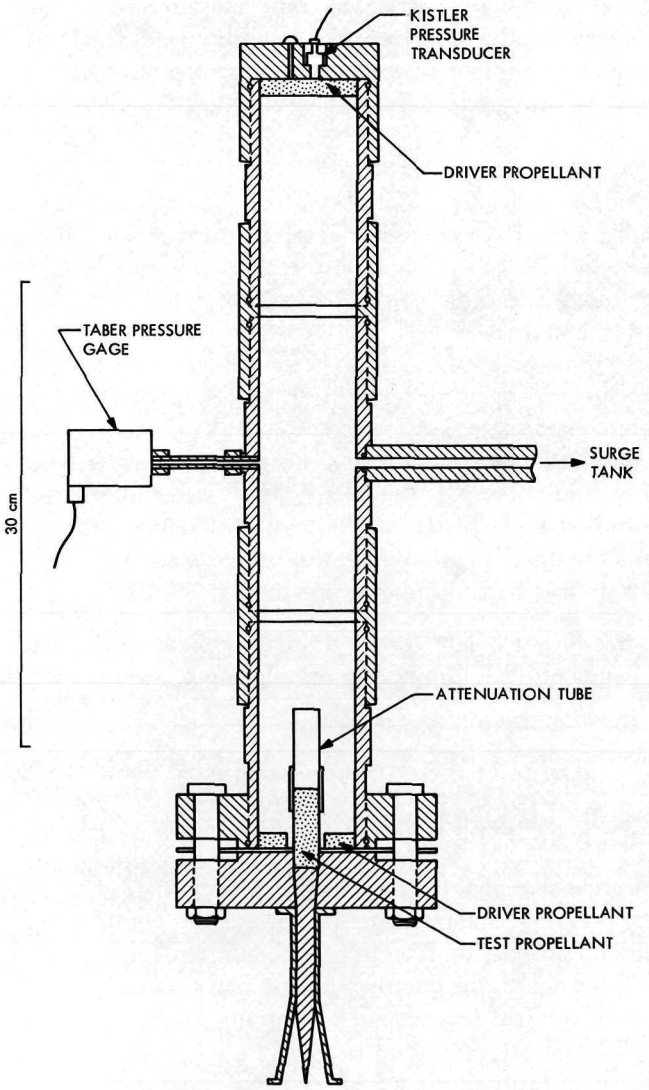

Fig. 14. T-burner cutaway drawing

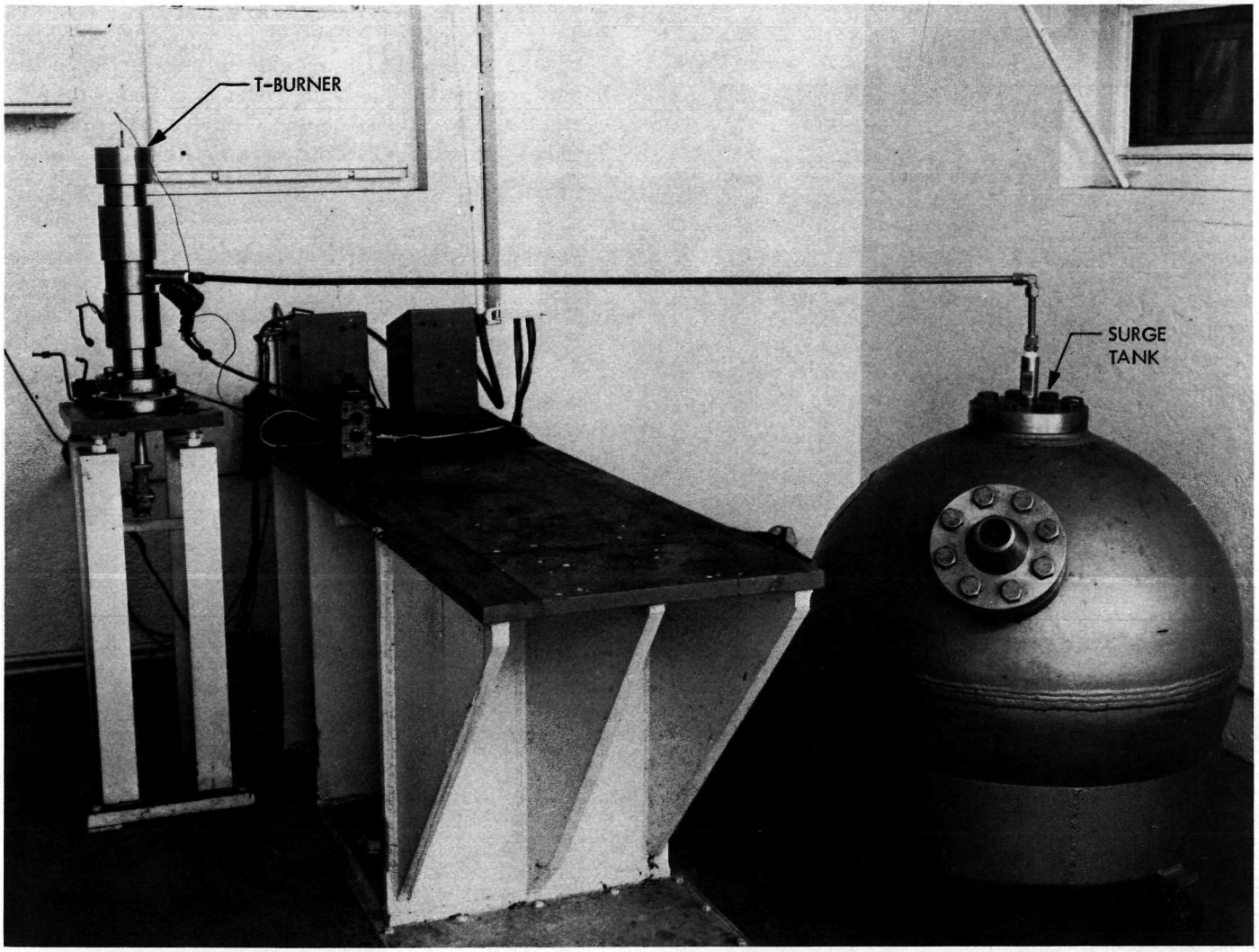

Fig. 15. T-burner test assembly

regression rate data for the four propellants, obtained in a conventional Crawford strand bomb, are shown in Fig. 16.

A majority of the tests were conducted using the first two propellants. The 540A formulation has been used extensively at JPL in combustion instability studies (Refs. 26 and 27). The CTPB propellant and a slightly modified version of it are based on a formulation used by investigators at the University of Waterloo in another effort to measure the transient regression rates of propellants undergoing rapid depressurization (Ref. 21). The regression rates of the JPL-mixed propellants were somewhat higher, probably due to different oxidizer size distributions. These latter two propellants were used primarily in the T-burner experiments.

A propellant, designated A-13,[1] which had been found to be very unstable in a number of prior T-burner studies (Ref. 26, as an example), was used as the acoustic driver propellant in the T-burner experiments. It is an ammonium perchlorate oxidizer propellant with polybutylacrylonitrile acrylic acid as the binder.

Dielectric constant measurements obtained for the 540A propellant are shown in Table 2.[2] The dielectric constant of the Melmac transition cone was 5.

---

[1]Generously supplied by the Naval Weapons Center at China Lake, California.

[2]Supplied by Professor S. V. Shelton, Georgia Institute of Technology, Atlanta, Georgia.

Table 2. 540A propellant dielectric constant measurements

Sample	Dielectric constant	Loss tangent
1	4.91	0.02
2	4.90	0.02
3	4.80	0.02

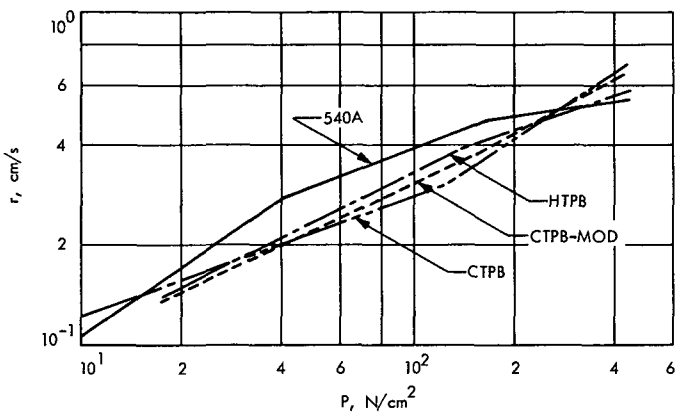

Fig. 16. Test propellant steady-state regression rate data

VI. Data Acquisition

The test data, consisting of the wave analyzer phase and amplitude output signals, filtered output of the operational amplifier, and pressure signals, were amplified and recorded directly on a CEC oscillograph. To get greater time resolution in a few T-burner experiments, the test signals were recorded on a 7-channel Ampex FR 600 tape recorder operated at a speed of 152.4 cm/s (60 in./s) and played back on the CEC oscillograph at a speed of 19 cm/s (7.5 in./s), resulting in an 8/1 expansion of the time scale.

VII. Test Procedure

Test procedures were basically the same for the two types of experiments. The ends of the propellant sample tubes were very carefully filed flush with the tube walls to reduce the reflection as much as possible from the propellant sample base. After the tube was screwed into the base plate (Fig. 17), a tuning operation was performed to minimize the magnitude of the fixed reflections in the system. A propellant-filled tuning tube of the same diameter as the test sample and 122 cm (48 in.) in length was connected to the free end of the propellant sample tube. Due to the lossy nature of the propellant, this tuning tube absorbed essentially all of the microwave radiation entering the propellant sample. Since the incident signal was completely absorbed, any reflection detected by the network analyzer was due to mismatches in the microwave system. The slide tuner was then tuned to cancel this reflected signal and the tuning tube removed. Typically, the fixed reflections were 70 dB or more below the reference signal amplitude after tuning.

The end of the propellant sample was then covered with a pyrotechnic paste[3] in which a nichrome wire was embedded (Fig. 18). In the T-burner tests the two discs of driver propellant were also coated with paste. A dried pellet of the paste embedded with a nichrome wire was then cemented to each disc, and the three sets of igniter leads were wired in parallel to the ignition power supply. In most T-burner tests the exposed portion of the sample tube below the female coupler (Fig. 14) was wrapped with glass tape to protect it from the flame of the lower propellant disc.

Following assembly, the bomb or T-burner surge tank was pre-pressurized with nitrogen to the desired level and the propellant sample(s) ignited. In the rapid depressurization tests the triggering circuit for the solenoid-controlled knife blade and nitrogen supply valve was activated after 2–3 cycles of the phase meter, when burning was well established and the chamber pressure stabilized.

VIII. Verification Tests

Several experiments were conducted to verify the spatial and time resolution of the regression rate measurement, the effect of propellant surface roughness on the measurements, and the accuracy of the system for quasi-steady-state regression rate measurements. In one test the propellant sample was replaced with a column of Dow-Corning oil with a dielectric constant similar to that of the propellant, and the phase shift was measured while fine droplets of oil were dropped on the oil column surface. The tests included dropping oil of two different viscosities from three different heights.

The test results showed features which would be expected if the apparatus were responding nearly instantly to the oil movement. Upon impact of the droplet,

[3]X-225, supplied by the Naval Weapons Center at China Lake, California.

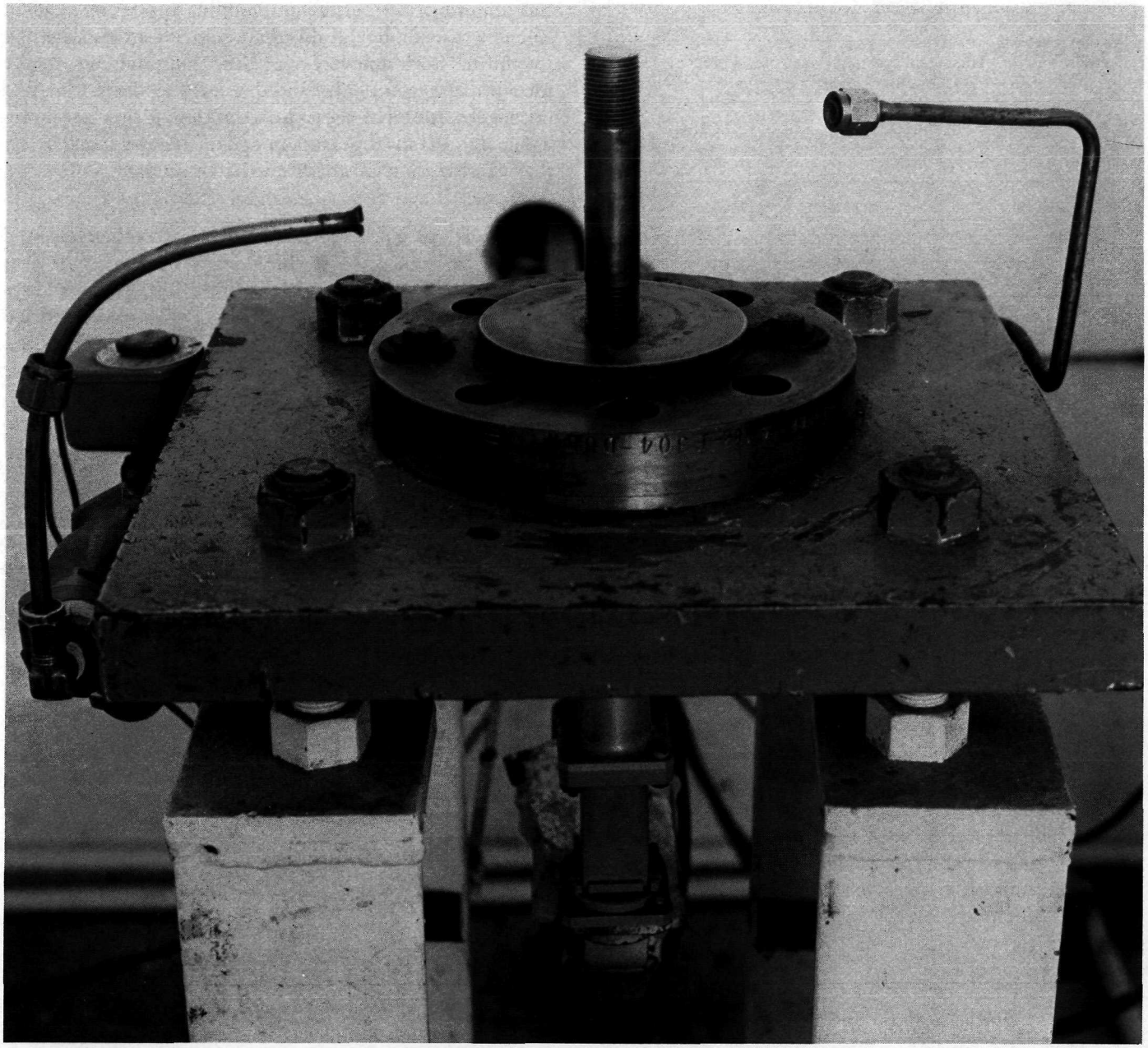

Fig. 17. Propellant tube mounted on microwave system base plate

there was an initial jump in the phase trace in the direction corresponding to a dynamic length increase. This initial jump was followed by oscillations in the phase trace. After the transient, the phase signal was shifted from its initial position by the amount expected from the change in surface level predicted from droplet size measurements. It was concluded from these tests that the experimental apparatus had a surface resolution of at least 50 μm (limited by minimum droplet size) and time response in the millisecond range.

In a second test, 400-μm crystals of ammonium perchlorate were dropped onto the surface of a partially filled propellant sample tube at varying positions on the surface. The tests verified that since the typical roughness scale of regressing propellants is much smaller than the microwave wavelength, the propellant surface still appears planar to the microwave signal.

A number of steady and quasi-steady regression rate measurements were obtained to check the accuracy of

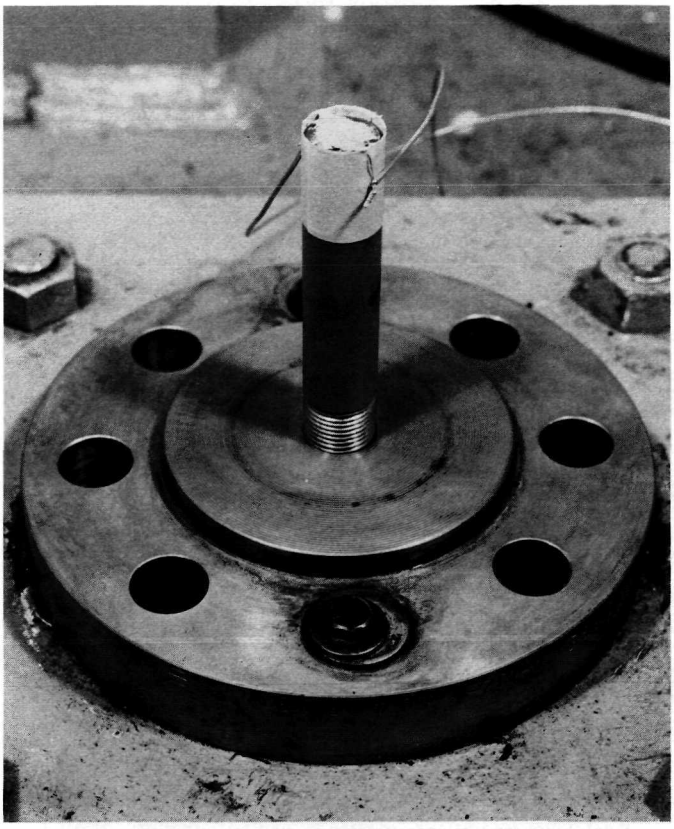

Fig. 18. Propellant tube igniter system

the instrumentation and theory. In the steady-state runs, the combustion bomb was pressurized to a desired level; the propellant sample was ignited and allowed to burn to completion at a relatively steady pressure.

Figure 19 is a representation of a segment of the oscillograph record from one such test for the 540A propellant. Depicted are the pressure, P, phase angle, ϕ, and the amplitude ratio of the reflected signal, A (the operational amplifier was not used in these early tests). Because the pressure was constant after the initial ignition transient, the linearity of ϕ and the magnitude of the oscillations of A provide a measure of how well the fixed reflections were tuned out. If only the burning surface reflection had been present, the phase channel would have a constant slope, and the amplitude would have gradually increased as a result of a decreasing propellant path length.

The amplitude channel exhibits an abrupt jump of approximately 2 dB immediately following ignition of the propellant sample. An amplitude increase of this magnitude or less after ignition was quite common, although usually not as abrupt. Static tests showed that mounting an empty 5.1-cm (2-in.) long tube on a propellant sample tube produced a 5-dB or larger increase in the amplitude of the reflected signal. It was concluded from these tests that the propellant surface itself is not a good reflector. Instead, as the propellant ignites and regresses down the tube, the hollow tube behind the surface cuts off transmission, and a larger portion of the incident radiation is reflected.

Although less than two phase cycles are shown in Fig. 19, there was a total of 13.2 for the entire 10.2 cm (4 in.) of propellant. The microwave wavelength in the propellant, λ_p, obtained from Eq. (7), was 1.55 cm.

Measuring the derivative of ϕ with respect to time for one cycle from Fig. 19, the calculated regression rate from Eq. (8) was 0.444 cm/s, which compares with a rate at this pressure of 0.470 cm/s from the Crawford bomb burning rate data. There was a slight progressivity of the regression rate over the complete run, probably due to heat conduction to the unlined metal walls of the propellant tube (see Fig. 22).

To measure the regression rate of a sample over a wide pressure range, the bomb was sealed after ignition, allowing the sample to pressurize the bomb as it burned. This pressurization can be considered quasi-steady, since pressurization rates were typically a few hundred N/cm²-s. No attempt was made to control the strand temperature. Test results for the 540A propellant are compared with the Crawford bomb data for the same propellant formulation in Fig. 20. Agreement during the initial portion of each test is reasonably good, but a progressivity with time in the microwave data is again apparent.

Compressibility effects of the propellant were investigated by subjecting a nonburning propellant sample to pressure transients equal to those imposed on the burning propellant samples. In these rapid depressurization tests, overall phase shifts of approximately 1 to 2 deg occurred, indicating propellant length increases of 20 to 50 μm. Such changes are in the same region with predictions based on the propellant bulk modulus. They cannot be considered insignificant. The net result is that the experimentally determined transient regression rates are the resultant of both a negative burning component and a positive or negative compressibility component (decreasing or increasing pressure), the magnitude of the

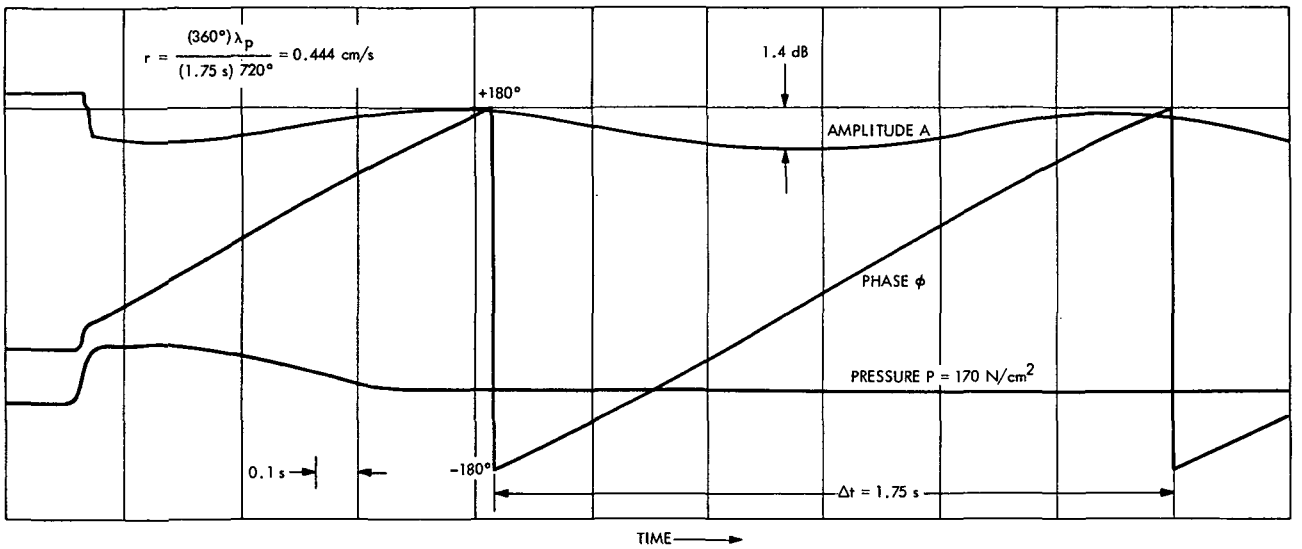

Fig. 19. Segment of oscillograph test record

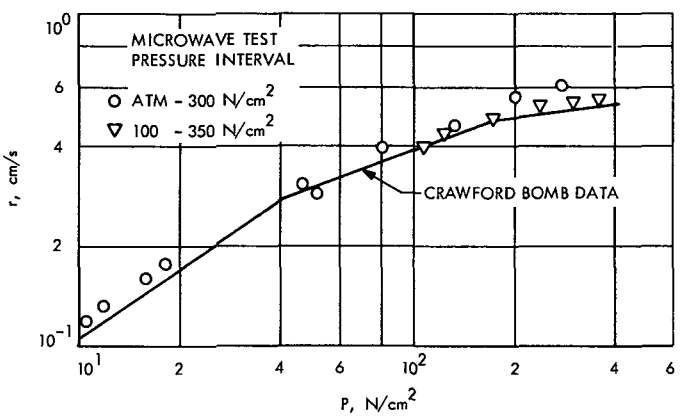

Fig. 20. Regression rate data comparison for 540A propellant

latter depending on the sample propellant length and physical properties and the test pressure and pressure gradient. Since the compressibility effect is real, and accurately adjusting the transient regression rate data to obtain the burning rate component would be a highly involved time-dependent process, no corrections were made to the data. It should be interpreted or utilized accordingly.

IX. Transient Regression Rate Measurements

A. Rapid Depressurization Tests

Figure 21 is a reproduction of the oscillograph record for a test resulting in extinguishment. The figure depicts the P, A, ϕ, and r signals. The pressure signal is from the Taber gage. Even with water cooling, thermal drifting of the Kistler gage was severe enough to necessitate setting the charge amplifier on short time constant, yielding an ac component measurement only. The principal value of this signal was as an accurate indication of the point of onset of depressurization. Since the initial response of the close-coupled Taber gage over the range of depressurization rates tested was found to be essentially equal to that of the Kistler gage, within the time resolution of the recorded data, use of the latter was discontinued early in the test program.

As the pressure drops from its initial value to atmospheric conditions, ϕ changes from a fixed constant slope to zero slope with respect to time. The oscillograph recorder was purposely operated at the relatively slow speed of 40.6 cm/s (16 in./s). This allowed a mean curve to be drawn through the electrical noise on the r signal, as shown. Although a higher recording speed gave better time resolution of the rapid pressure decay, it became very difficult to differentiate between noise and any real oscillations in the r signal.

In a majority of the tests, the bomb pressure prior to venting, P_0, was in the 210- to 270-N/cm² range. The 350 N/cm²-rated burst diaphragms that were generally used would not rupture cleanly at pressures below 200 N/cm². For the 540A propellant a few tests were run at bomb pressures near 140 N/cm² using 200 N/cm²-rated burst diaphragms.

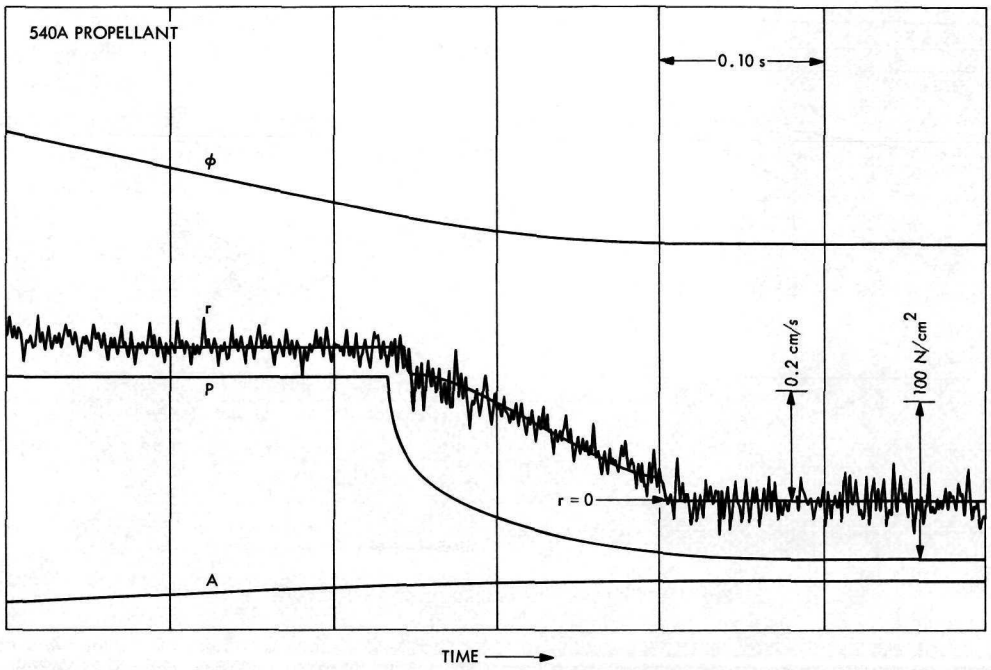

Fig. 21. Rapid depressurization oscillograph test record

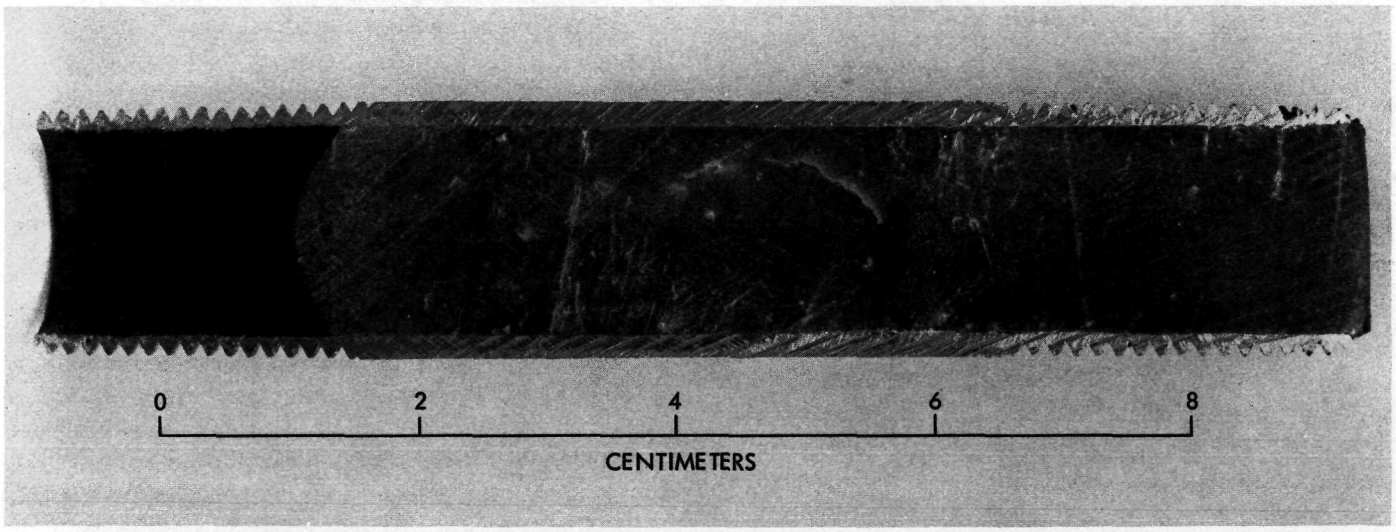

Fig. 22. Sectioned view of typical rapid depressurization-quenched propellant sample

A sectioned view of a typical quenched propellant sample is shown in Fig. 22. The propellant developed a convex surface due to increased regression at the tube wall. Since the surface irregularity is much smaller than λ_p, the surface appears planar to the microwave signal.

1. 540A propellant. Figure 23 shows the test results for two tests at initial pressures in the 140-N/cm² region. Shown are the bomb transient pressure, the propellant steady-state regression rate at the corresponding pressure, and the measured regression rate, each normalized by the initial value at the time of onset of depressurization. As shown, for each test there was a lag of about 10 ms in the response of the measured regression rate to the depressurization, followed by an abrupt drop to 0.8 to 0.9 of its initial value. The rate then leveled off and continued to steadily drop at a decreased rate. In Fig. 23a, it leveled off at the atmospheric pressure rate after ap-

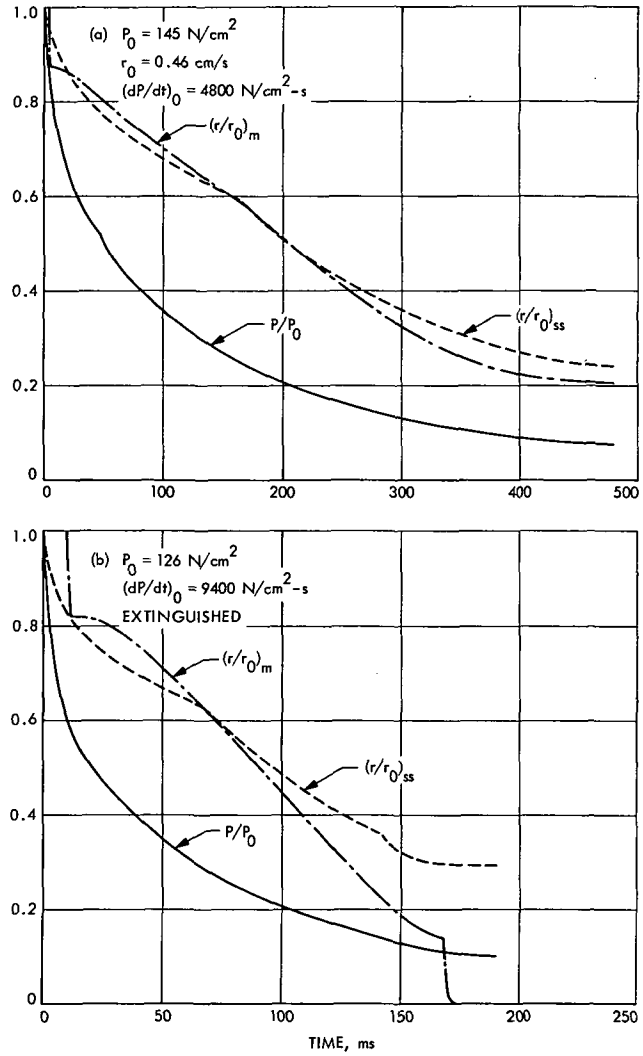

Fig. 23. Rapid depressurization experimental data for 540A propellant: initial pressure of approximately 140 N/cm²

proximately ½ s. With a larger diameter venting orifice, the rate in Fig. 23b decreased for approximately 170 ms, then abruptly dropped to zero.

The normalized test results for six tests with an initial pressure in the 230- to 270-N/cm² range are shown in Fig. 24. The tests are shown in the order of ascending rate of depressurization. Figure 24c was an anomaly in that nitrogen flow continued into the bomb after rupturing of the diaphragm. This resulted in a very slow pressure decay over the latter portion of the vent, considered to be the critical region for extinguishment (Ref. 6, for example). As discussed earlier, the slow recorder speed made accurate determination of the higher initial rates of depressurization impossible. The values quoted are very approximate.

Except for the initial lag period, the measured regression rate generally fell below the steady-state value. This initial lag diminished and eventually disappeared with increasing rate of depressurization. Figures 24a and 24c did not extinguish, but slowly recovered to the atmospheric pressure burning rate approximately ½ s after the onset of depressurization. Figures 24b, 24d, and 24e all extinguished, with the regression rates smoothly going to zero rather than suddenly terminating. With the largest venting orifice (Fig. 24f), the regression rate abruptly dropped to zero, undershooting it before leveling off to zero. Calibration checks showed no such instrumentation undershoot to an abrupt change in ϕ. A possible explanation for this apparent negative regression rate will be discussed in *Section IX-C*.

Beginning with Fig. 24b, the measured regression rate exhibited rather irregular oscillations which were not evident in the pressure signal. (However, the response time of the chamber was too great to readily discern any pressure variations caused by the regression rate oscillations.) The amplitude of the oscillations increased with increasing rate of depressurization, becoming pulse-like in Fig. 24d, and then diminished (Fig. 24e) and disappeared (Fig. 24f) as the rate of depressurization increased, and combustion extinction became more positive. The oscillation frequencies were roughly below 100 Hz, and appeared to have a general trend of decreasing with decreasing rate of depressurization.

2. HTPB and CTPB propellants. Test results for the HTPB and CTPB propellants are shown in Figs. 25 and 26, respectively. The results for the two polybutadiene (PB) binder system propellants were quite similar and differed significantly from the polyether-polyurethane (PU) binder 540A results. The initial rates of depressurization required to terminate combustion were greater than twice that found for 540A. Also, the regression rate behavior of the HTPB and CTPB propellants generally seemed more "sluggish." The lags in the initial response of the regression rate to the depressurization were about double that of 540A and persisted up to the highest depressurization rates tested. In the no-quenches the regression rate would oscillate once, drop off almost to zero, and slowly recover and continue at a low rate. The Fig. 26b test results, as can be seen, were rather unusual. After approximately 70 ms of no measurable regression rate, regression slowly resumed and leveled off at a rate considerably below the steady-state value for atmospheric pressure. Approximately 70 ms later, the r signal exhibited a strong spike, as if some material had been violently removed from the surface, and then dropped

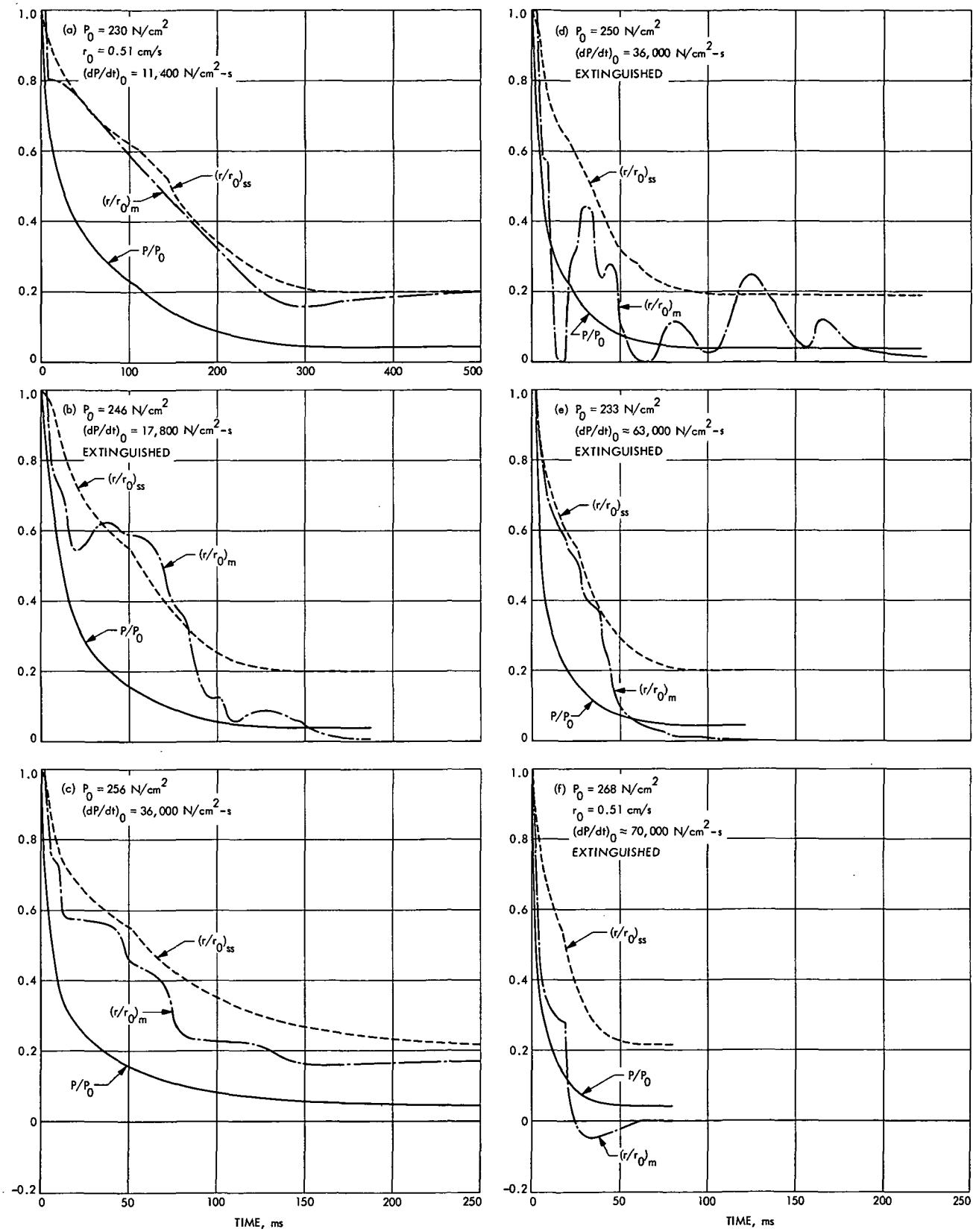

Fig. 24. Rapid depressurization experimental data for 540A propellant: initial pressure of 230 to 270 N/cm²

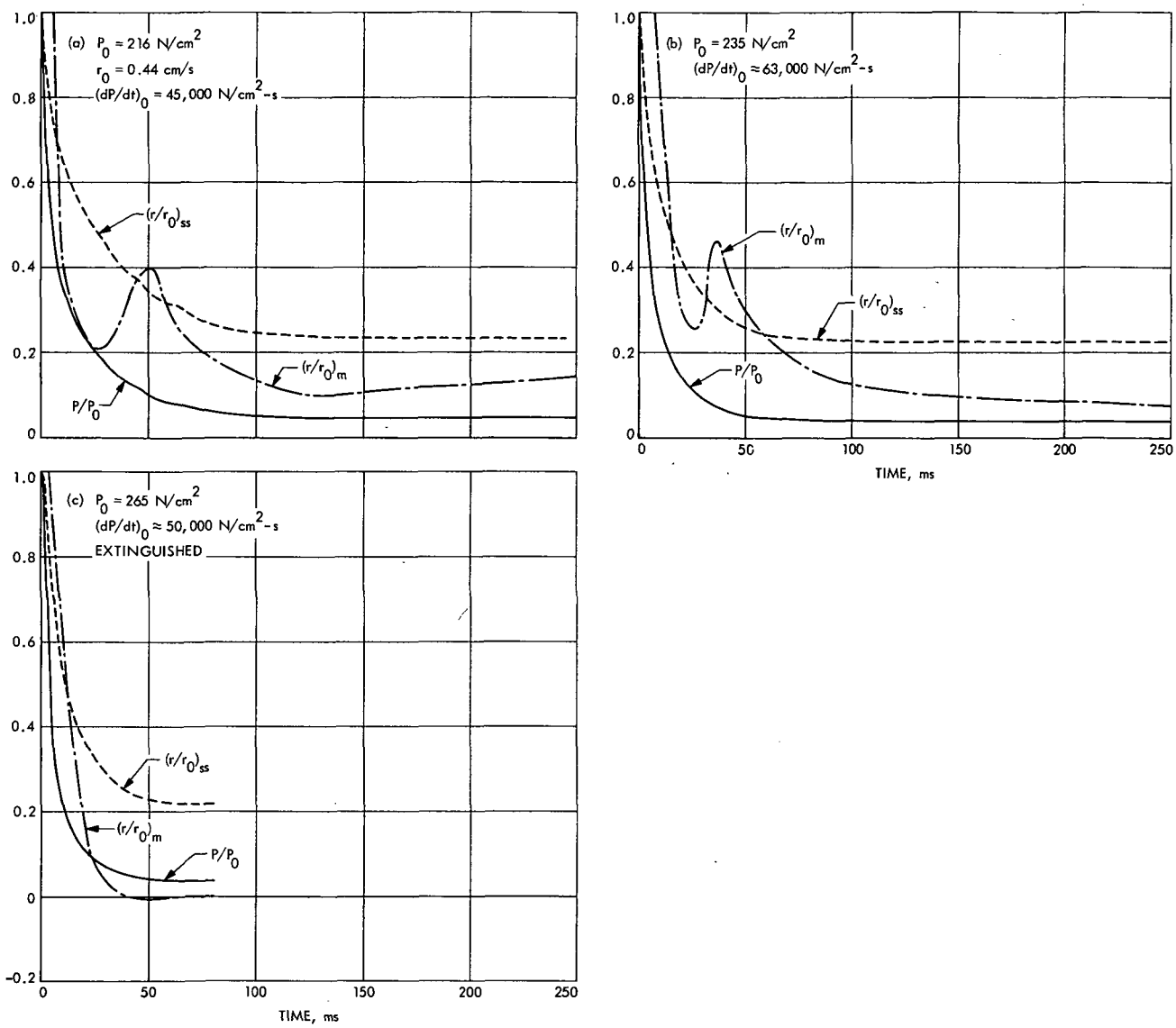

Fig. 25. Rapid depressurization experimental data for HTPB propellant

permanently to zero. Examination of the extinguished burning surface did not reveal any unusual appearance.

3. *Measurement errors.* Two possible sources of error in the regression rate data were (1) the drawing of a mean curve through the r channel noise (Fig. 21), and (2) correcting the ϕ and r signals for fixed reflections in the microwave system. The maximum uncertainty in regression rate due to averaging the noise was estimated at 0.01 cm/s, a possible error of a few percent. As stated earlier, corrections for fixed reflections were only necessary for the very gradual depressurization experiments (Figs. 24a and 24c, for example). In general the corrections did not exceed 3–4%.

Not enough data under closely controlled test conditions (P_0, $\dot{P}_0$, etc.) were obtained to make any definite claims concerning the reproducibility of the results. Because of the short duration of the tests, there was not sufficient time to accurately control the bomb pressure by manual means after initial pressurization and ignition of the propellant strand. The initial rate of depressurization was also difficult to reproduce. This was probably related to how cleanly the burst diaphragm ruptured.

4. Comparison with existing data. As mentioned earlier, the only other transient regression rate data currently available is that of Yin and Hermance (Ref. 21). The method of measurement consisted of using a solid-

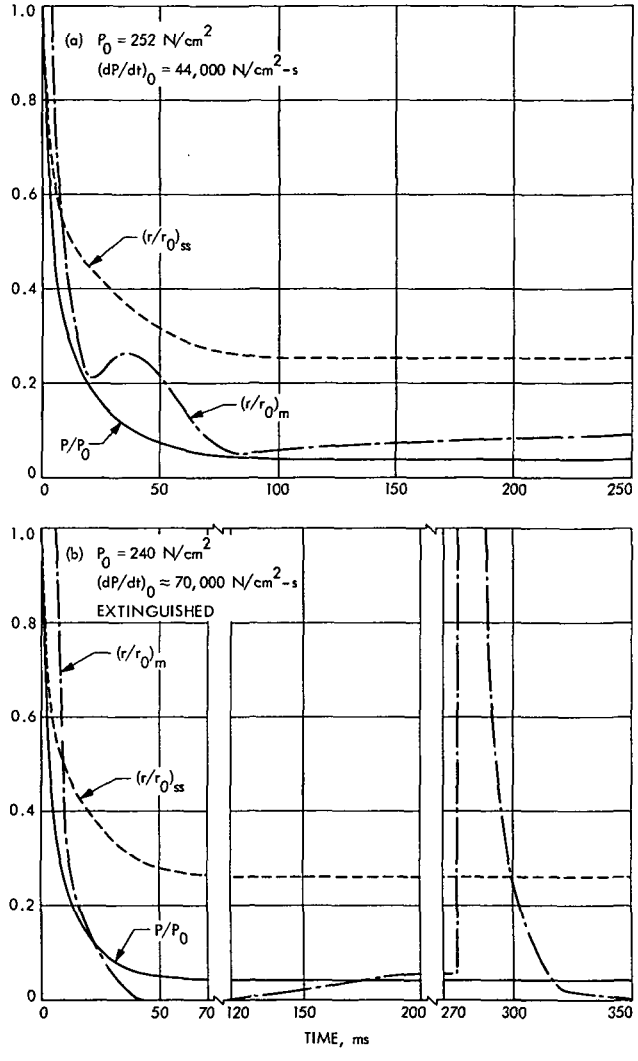

Fig. 26. Rapid depressurization experimental data for CTPB propellant

propellant strand 0.635 × 0.635 × 5.1 cm (¼ × ¼ × 2 in.) as the dielectric material of a capacitor forming a part of an L–C tuned circuit in an electronic oscillator. The capacitance and resonant frequency of the oscillator varied directly with change in propellant length. The frequency variation was converted into a voltage and differentiated electronically to obtain a voltage directly proportional to the propellant regression rate. The effect of flame plasma on capacitance was reportedly subtracted out electronically.

Rapid depressurization experiments were conducted in a rarefaction tube, with the propellant sample at one end and a diaphragm at the other. Reference 21 reported results obtained using a propellant with the same formulation as the CTPB propellant of the present study. Tests

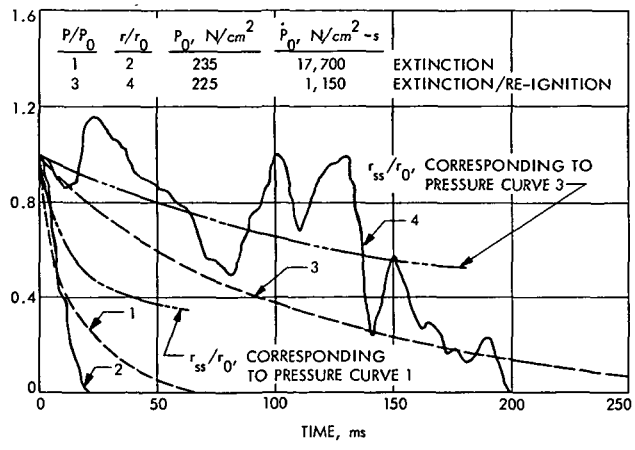

Fig. 27. Rapid depressurization experimental data for HTPB propellant, Ref. 28

have also been carried out using the HTPB propellant of this study (Ref. 28).

A comparison of the transient regression rate data from the two experiments is hindered somewhat by the large differences in the geometries of the two combustors and the resulting differences in the experimental transient pressure conditions. (See Refs. 6 and 29 for discussions of the effects of motor geometry on solid-propellant rapid depressurization phenomena.) For similar initial pressure conditions, decay to atmospheric pressure was more rapid in the Yin–Hermance device (compare Fig. 27 with Fig. 24b), and combustion extinguishment was obtained under significantly lower overall depressurization rates. The initial depressurization rates reported by Yin–Hermance are therefore considerably lower than those of the present study. Propellant compressibility effects (*Section VIII*) were also not necessarily the same in the two experiments, due to the different sample geometries and methods of holding the test samples.

The transient regression rate data from the two experimental systems exhibited several similar characteristics: (1) a delay in the response of the regression rate following the onset of depressurization, (2) low-frequency oscillations in the decreasing regression rate not evident in the chamber pressure, and (3) an increase in frequency and decrease in amplitude of the oscillations with increasing rate of depressurization.

Even attempting to take into account the differences in the two combustors, several fundamental discrepancies between the respective data still seem to exist: Yin and Hermance reported their transient regression rates to be greater than the steady-state rate at the corresponding

pressure until extinction occurred. In the present study this generally was the case only early in the depressurization at the lowest rates tested. In tests using (a) a propellant with the same formulation as that used by Yin and Hermance (CTPB), and (b) the same propellant (HTPB), the JPL results did not exhibit the low-frequency oscillations of the Yin–Hermance transient rate data (Fig. 27). Instead the measured rates exhibited a characteristic S-shape (Figs. 25 and 26).

The regression rate data seem to generally agree with the previously summarized findings of Steinz and Selzer (Ref. 10) and others: (1) at depressurization a brief delay followed by rapid and complete extinguishment of the flame for sufficiently large depressurization rates; (2) for lower rates a recovery and persistance of the flame until near the end of the pressure transient, where the flame then either begins to recover or extinguishes; and (3) irregular burning of the recovered flame near the critical depressurization rates for extinguishment. The lower than steady-state predicted regression rates of the PB binder propellants following the pressure transient could be due to only partial recovery of this secondary flame; i.e., the flame had not yet spread over the entire burning surface.

B. T-Burner Tests

A total of 20 tests were performed with the 4 test propellants. The surge tank pre-test pressure in about half of the tests was approximately 180 N/cm^2. This gave a mean T-burner pressure during the test of 220–230 N/cm^2 and gave the strongest limiting pressure oscillations (45 N/cm^2 peak-to-peak and greater). For overall amplitudes greater than 70 N/cm^2 the basically sinusoidal waveform began to exhibit distortions due to higher harmonic frequencies, degenerating, in the extreme, to a sawtooth-type wave for one test with 140-N/cm^2 oscillations.

The Dranetz Phase Meter and differential amplifier were not used in the first 13 tests. For these tests, regression rate data had to be deduced from the phase information.

For the first half of the tests, the results were quite similar. The A and ϕ signals contained both high-frequency oscillations approximately in phase with the pressure, and erratic low-frequency (100 Hz and less) oscillations of much greater amplitude (Fig. 28). The amplitudes of both types increased with the magnitude of the pressure oscillations, the high-frequency ϕ oscillations being difficult to differentiate from the Hewlett-

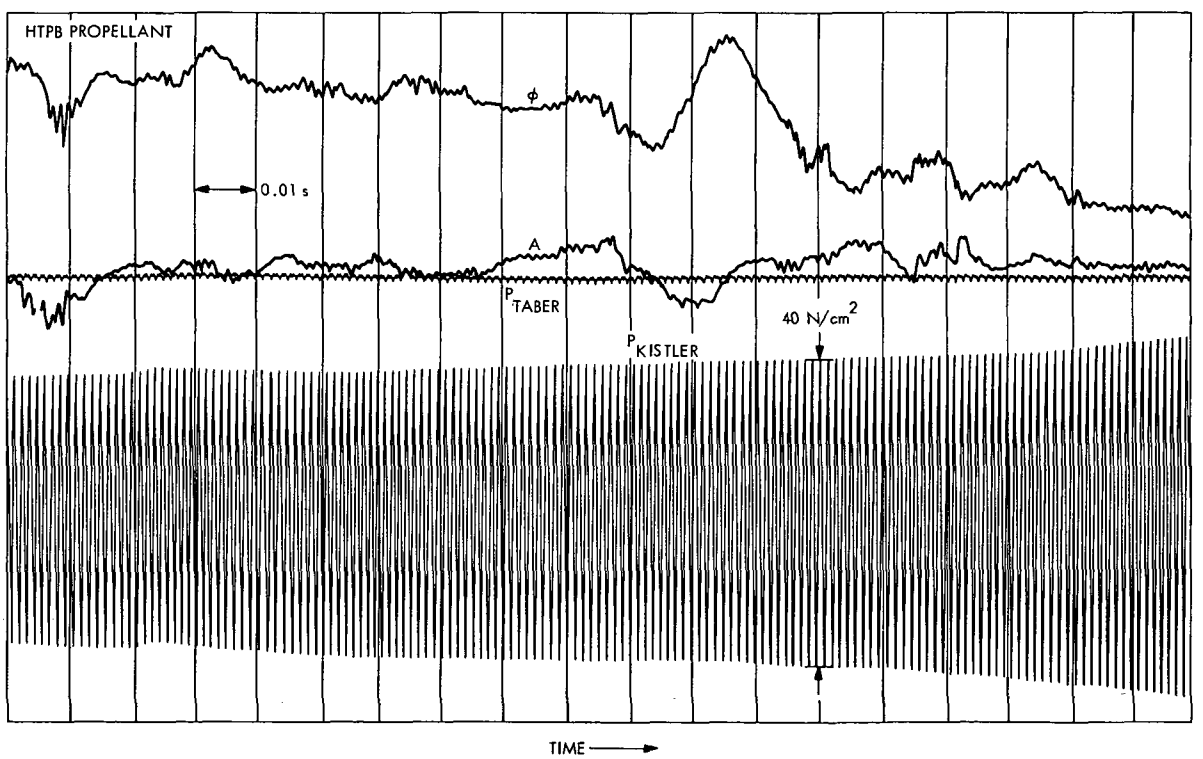

Fig. 28. T-burner oscillograph test record: high- and low-frequency oscillations in phase and amplitude

Packard Phase-Gain Indicator signal noise at the lower magnitudes.

The regression rate amplitudes, r', determined from the high-frequency ϕ oscillations, were 30 or more times greater than the measured mean regression rates, $\bar{r}$; completely unreasonable values. The phenomenon causing the low-frequency oscillations was also a mystery. It was known, based on the results of previously described tests, that the propellant–gas interface itself was not a strong reflector. Therefore, the low-frequency oscillations were first postulated to occur as a result of the beating together of reflected waves from the flame zone as well as the propellant surface. Later, it was noticed that on a few tests the low-frequency oscillations disappeared shortly *before* burnout and acoustic decay of the T-burner. It was then postulated that the T-burner itself was acting as a waveguide for any transmitted microwave signal, a portion of which was being reflected off of the burning T-burner propellant surface and transmitted back into the microwave propellant strand. When the empty tube above the propellant strand became long enough to become a complete short, the low-frequency oscillations would disappear. Subsequent tests proved the latter argument to be the correct one.

A 5.1-cm (2-in.) extension tube was coupled to the propellant strand (Fig. 14) in all subsequent tests. This eliminated the low-frequency oscillations and diminished the amplitude of high-frequency oscillations (Fig. 29). The latter was only positively distinguishable from instrumentation noise in the parts of the signal cycle where noise was largely absent. The reduced regression rate amplitudes were still unreasonable, one to five or more times the measured mean values. The high-frequency oscillations did not seem to be present during the entire burn time of the T-burner. They would appear and then disappear. In a few tests, no high-frequency oscillations were detectable, although the T-burner oscillated in its normal fashion.

The r signal test information obtained after the addition of the Dranetz Phase Meter and differential amplifier to the microwave system agreed with the previous results (Fig. 30).

The first two tests after incorporation of the propellant extension tube used CTPB test propellants. The final eight tests in the series used 540A and HTPB propellants. An anomaly, consisting of a large increase in the measured mean regression rate of the propellant sample, to values of 2.5 to 12 cm/s, was observed in five of these tests. These high rates were corroborated by the total burn time of the propellant samples. The T-burner failed to develop any acoustic pressure oscillations in two of the three tests where the anomaly did not occur. Onset of the run-away regression generally occurred somewhat abruptly after approximately a ½- to 1-s duration of normal burning (Fig. 31). In most tests the regression rate returned to normal for about the last ϕ cycle prior to burnout of the sample. Burnout of the sample occurred before or shortly after that of the T-burner.

The rapidly varying phase test signals had the same appearance as that of the very first test in the series, when no thermal protection was provided to the sample tube, and it melted through near its base. It was conjectured that the propellant near the tube wall was being heated sufficiently to greatly increase the regression rate in this region and, consequently, the propellant burning area. Therefore, in the latter three tests in the series, the thickness of glass tape applied to the propellant sample tube was increased (up to approximately 0.3 cm) in an attempt to better insulate the tube from the oscillating hot driver-propellant gases. The accelerated regression continued, occurring in two of the three tests. The attenuation tube and its coupler (Fig. 14) were not protected, and could possibly have conducted heat back to the propellant sample. Heating of the extension tube by the test sample flame itself might also have been a contributing factor. Although the problem was not resolved, external heating of the propellant sample seems to be the most reasonable explanation for the anomaly.

The phase angle relationship between the P and r test signals could be obtained from the Ampex tape-recorded data (Fig. 30). The measured phase difference between the two signals was roughly 90 deg. Correcting for the phase shift of the differential amplifier (Fig. 9), the phase lead of r over P was 60 deg.

C. Plasma Effects Analysis

Two findings make the experimental results somewhat suspect: (1) at the maximum depressurization rates tested, the r signal dropped to negative values (Figs. 24f and 25c); and (2) in T-burner tests, the amplitudes of the r signal oscillations generally equaled or exceeded the mean regression rates. Such high response would be more indicative of gaseous rather than solid phase fluctuations.

The primary assumption made in deriving Eq. (6) was that the phase change at the burning propellant surface was essentially constant. Thus, it became of no importance when the total phase difference was differentiated.

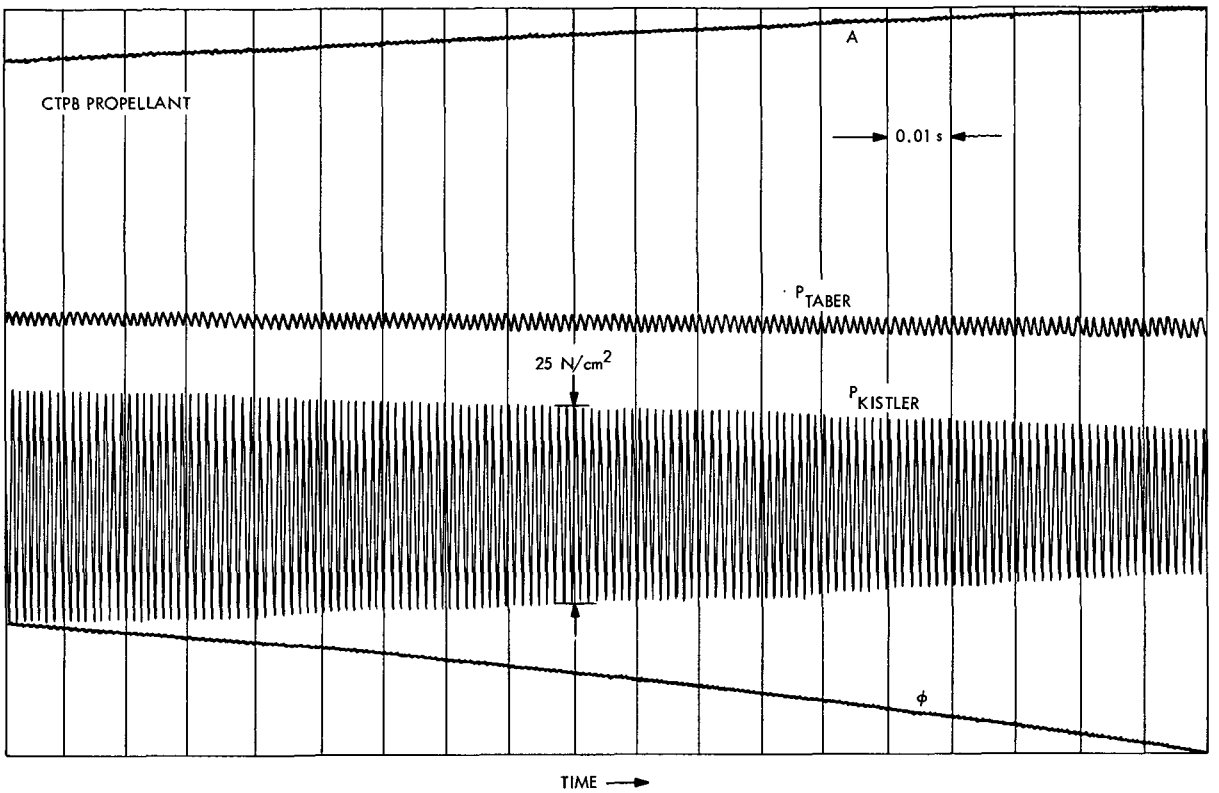

Fig. 29. T-burner oscillograph test record: 5.1-cm extension added to test propellant tube

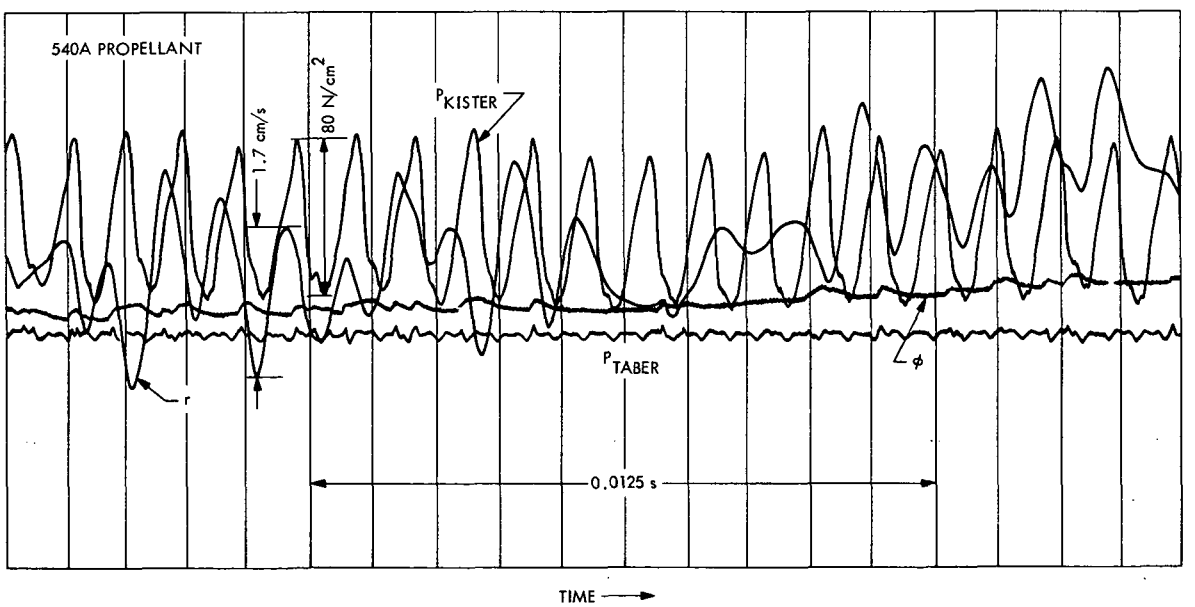

Fig. 30. T-burner oscillograph test record: incorporating r channel

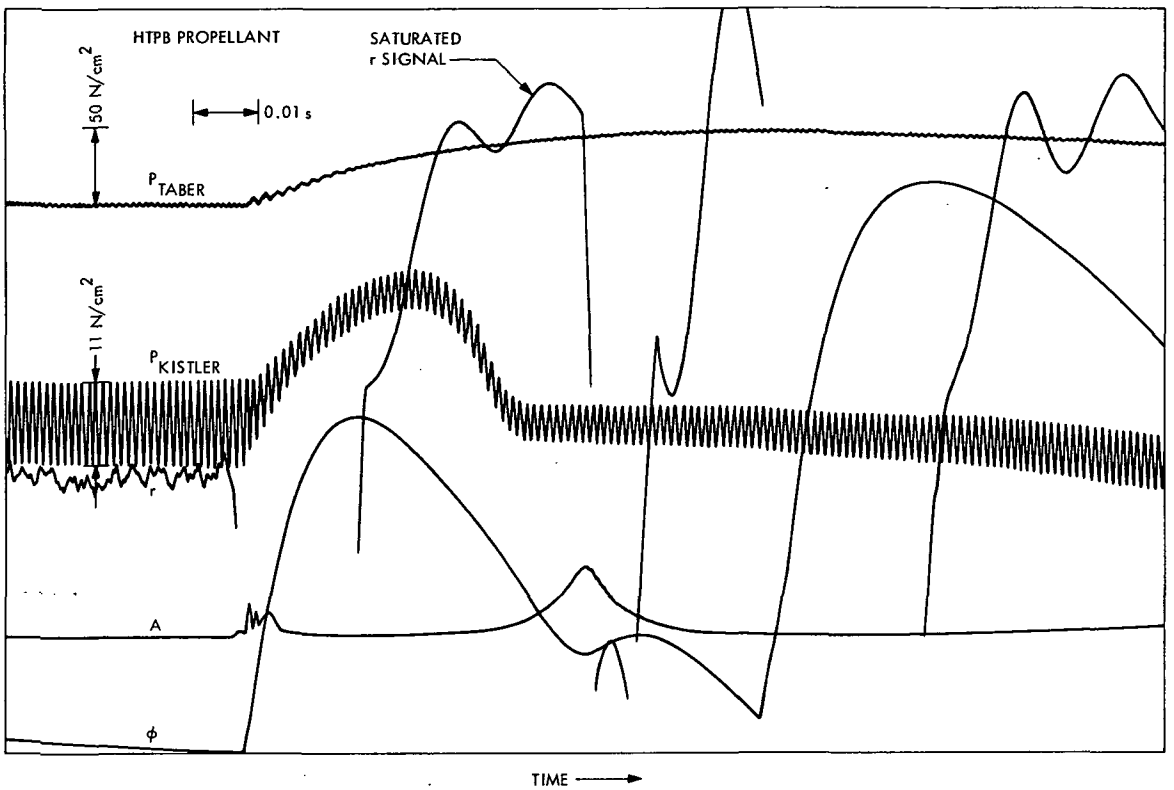

Fig. 31. T-burner oscillograph test record: abrupt increase in test propellant burning rate

As pointed out by Plett and Summerfield (Ref. 30) in a recent analysis of the effect of flame zone ionization level on the microwave measurement of solid-propellant transient burning rates, this assumption is not necessarily valid for transient combustion. Due to transient plasma concentrations, the phase change at the surface can vary significantly with changes in pressure. During periods of rapid pressure transients, these phase changes over short time intervals contribute substantially to the apparent regression rate.

Plett and Summerfield calculated an apparent propellant regression rate, as measured by the microwave phase shift technique, including both the Doppler shift (the actual burning rate) *and* a propellant/plasma interface phase shift caused by transients in the flame zone ionization level. To obtain a possible indication of the magnitude of this effect in the present experiments, parametric calculations were carried out for several simulated test conditions using a modified version of the analytical procedure of Plett and Summerfield.

In Ref. 30 Plett and Summerfield treated the flame zone as an unbounded region with microwave propagation properties determined solely by the ionization level of the flame gases. Because of the metal tube which contained the propellant sample and enclosed the flame zone as the sample burned, the region above the burning propellant surface in the present experiment is more properly treated as a dielectric-filled circular waveguide. A tube with an inner diameter of 1.27 cm was used for calculation purposes. This small guide significantly alters wave properties. Also, in Ref. 30, the plasma generated by the propellant flame was assumed to be incident to the propellant itself. This may not be the case. In the simplified combustion model of Culick and Dehority (Ref. 31), a transition zone is included between the propellant and the actual flame. In this region propellant is in a gaseous phase, but has not yet undergone combustion. Since little is known about the dimensions of this zone, varying values were used in the calculations.

Details of the analytical procedure used are given in the *Appendix*. The following expression was derived for the normalized apparent regression rate:

$$\frac{r}{r_0} = \left(\frac{P}{P_0}\right)^{0.415} + \frac{\dot{\phi}_s}{202°/\text{second}} \tag{9}$$

where the first term on the right hand side is the assumed actual regression rate and the second term is the spurious

contribution resulting from the variation with pressure of the flame zone plasma density.

The calculations were carried out for 3-cm microwaves, allowing the results for $d = 0$ to be compared directly with those of Plett and Summerfield. The microwave constants of the experimental microwave regression rate apparatus were somewhat different, but the calculated results for the two sets of constants would be very similar.

1. Rapid depressurization calculations. The results for two sets of rapid depressurization calculations will be discussed here. The following expression was used for the transient pressure:

$$P(\text{atm}) = 1 + (P_0 - 1)e^{-bt} \tag{10}$$

For a P_0 of 20 atm, b values of 66.67 and 1000, respectively, were chosen to correspond approximately to the lower and upper depressurization rate limits of the experimental data.

The mole fraction of ionizable species, Y (simulated by sodium in these calculations), was varied by factors of 10 from 10^{-8} to 10^{-6}. At the initial pressure of 20 atm, values of 0, 0.001, and 0.01 cm were assumed for the initial width, d_0, of the transition zone. The zero value was for comparison to Plett and Summerfield's calculations. The other two values were chosen to correspond roughly to the range of values described by Culick (Ref. 31).

The calculated apparent regression rates for the two transient pressure histories and the assumed values of Y and d are compared with the assumed actual profiles in Figs. 32 and 33. As might be expected, the general shape of the curves are quite similar to those obtained by Plett and Summerfield. Specific values, however, are significantly different. As was found by Plett and Summerfield, the analysis predicts that the use of microwaves to measure transient regression rates only gives accurate results when the propellant has a very low concentration of easily ionizable metals.

The results for $d_0 = 0.001$ cm are almost identical to those for $d = 0$. Although minor differences are apparent, a transition zone of this small dimension is clearly insignificant. However, the calculations with $d_0 = 0.01$ cm show a marked change. During depressurization, the width of the transition region was assumed to increase according to the expression

$$d = d_0(P_0/P) \tag{11}$$

As might be expected, this increase in the transition region gives an apparent increase in strand length, corresponding to an apparent drop in the regression rate.

Comparing the calculations with the depressurization experimental results yields several obvious differences. The initial abrupt increase in the apparent regression rate calculated for $Y = 10^{-6}$ was not observed experimentally. For the magnitude of depressurization used in the first calculation, $(dP/dt)_0 = 12{,}800$ N/cm²-s, the experimental results would predict that the measured regression rate should equal or be less than the quasi-steady-state predicted value (Fig. 24a). The analysis is in agreement only if the concentration of easily ionizable metals is less than 10^{-7}.

As one would expect from the model, at the higher depressurization rate, $(dP/dt)_0 = 64{,}200$ N/cm²-s, the variations in apparent burning rate became more exaggerated. The results for $Y = 10^{-7}$ were quite interesting; the burning rate abruptly dropped initially and exhibited a single oscillation of 83 Hz frequency. A single oscillation, but at a lower regression rate level, was observed in the experimentally determined regression rates in this depressurization rate range for the PB binder propellants (Figs. 25 and 26). But with further increase in the rate of depressurization, the two trends differ in that the amplitude of the experimental oscillations diminished and eventually disappeared, whereas, as shown, the theory predicts the opposite. Again, a low propellant concentration of easily ionizable metals seems to be indicated.

2. T-burner calculations. Pursuing the problem further, plasma effects calculations were carried out using the following sinusoidal pressure input to simulate T-burner test conditions:

$$P(\text{atm}) = 15 + 1.5 \sin [2\pi t\,(\text{ms})/1.2] \tag{12}$$

This corresponds to a frequency of 830 Hz and a peak-to-peak amplitude of 31 N/cm², conditions similar to those at which fluctuations in the measured regression

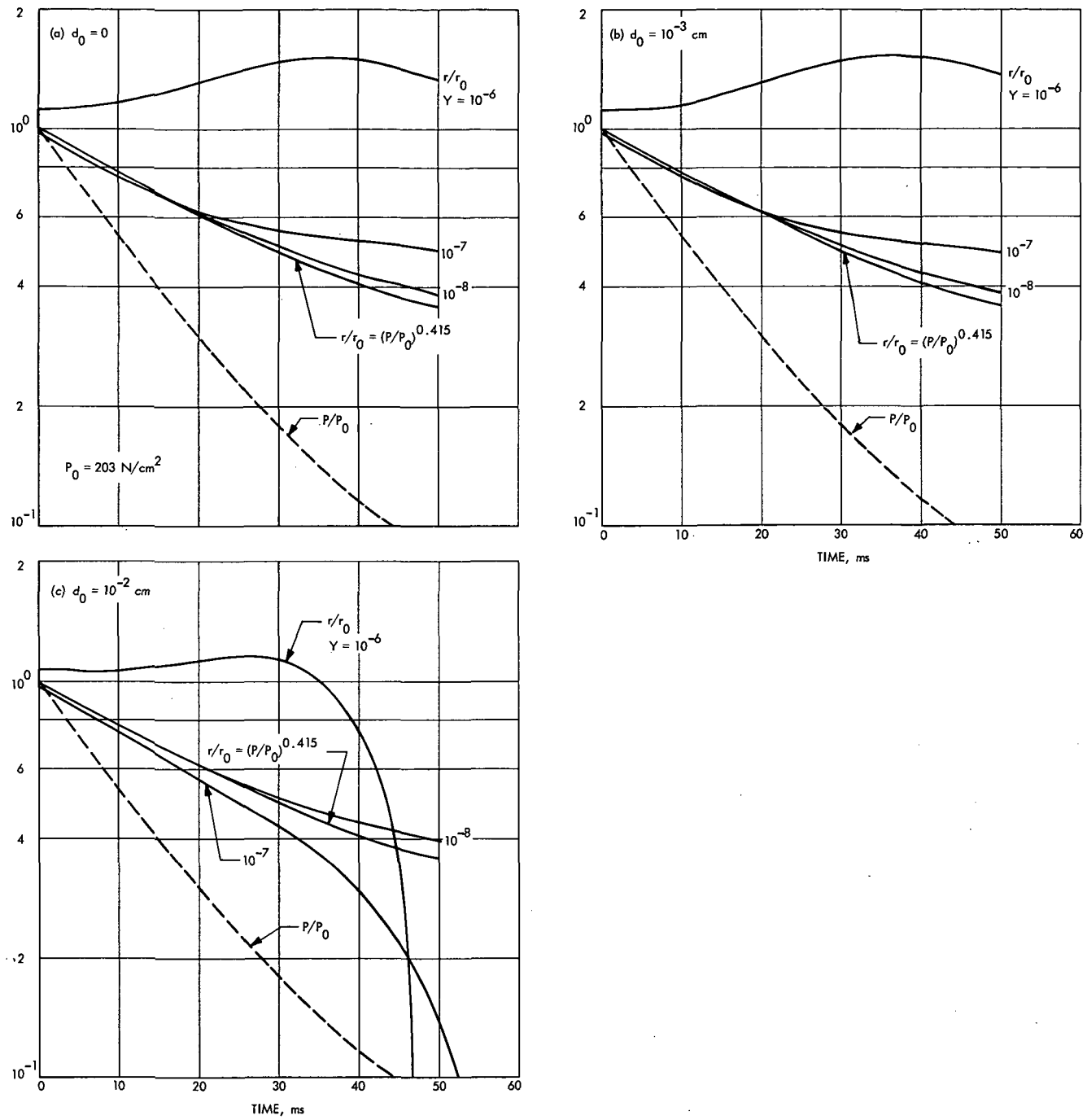

Fig. 32. Results of apparent transient burning rate calculations: initial depressurization rate = 12,800 N/cm²-s

rate were observed in two of the latter T-burner tests with propellant extension tubes. Y values were again varied by factors of 10 from 10^{-8} to 10^{-5}. A single initial flame stand-off distance of 10^{-3} cm was assumed.

The results of the calculations, shown in Fig. 34, were again very sensitive to Y. For $Y = 10^{-8}$, the apparent oscillatory regression rate was almost identical to the assumed actual value, giving an $r/\bar{r}$ amplitude of 1.04. For increasing Y, $r/\bar{r}$ amplitudes of 1.16, 3.25, and 21.3 were obtained for Y values of 10^{-7}, 10^{-6}, and 10^{-5}, respectively ($r'/\bar{r}$ values of 0.16, 2.25, and 20.3). Also, interestingly, the calculations predict an increasing apparent burning rate phase lead with increasing Y, equaling approximately 75 deg for $Y = 10^{-7}$.

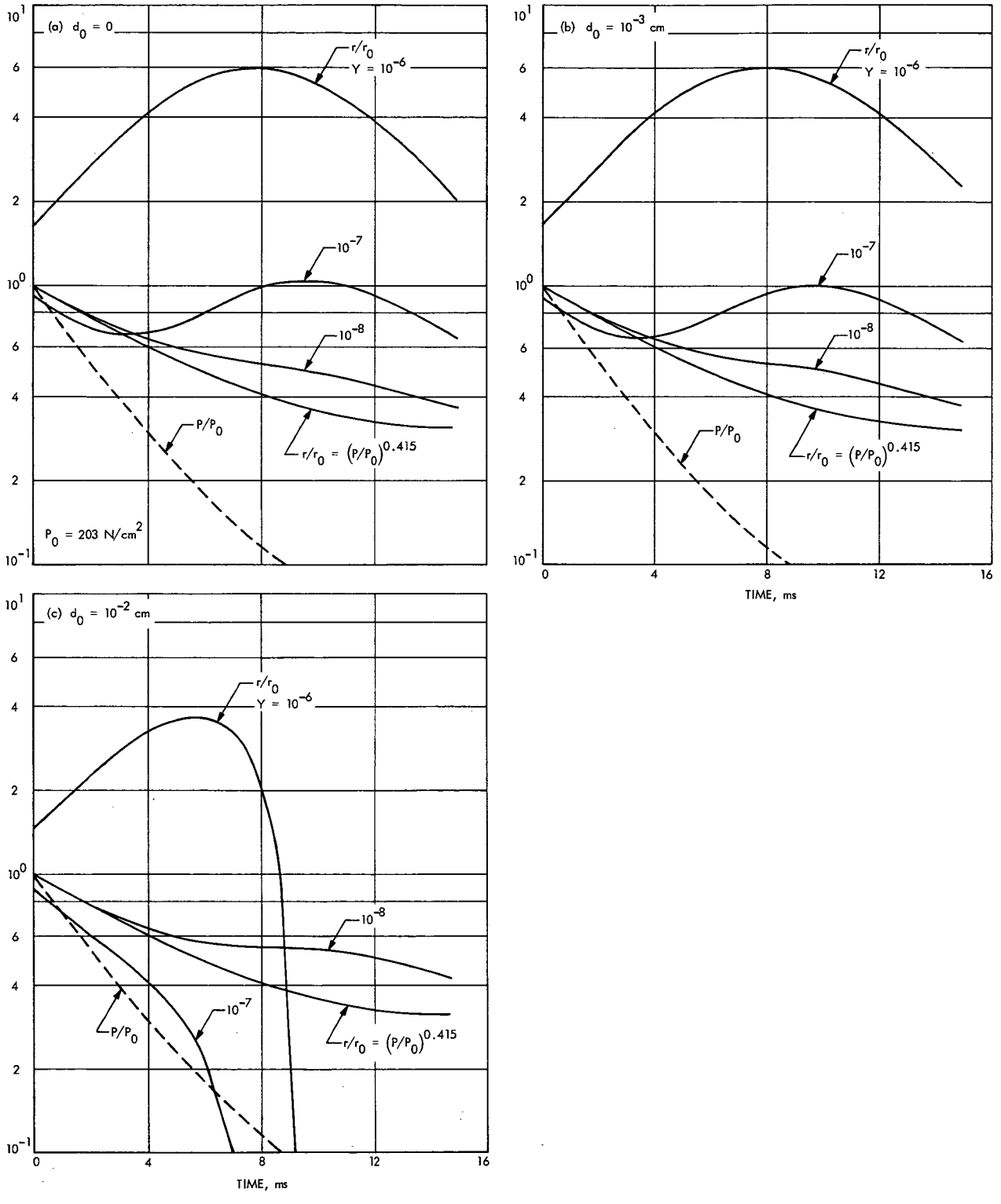

Fig. 33. Results of apparent transient burning rate calculations: initial depressurization rate = 64,200 N/cm²-s

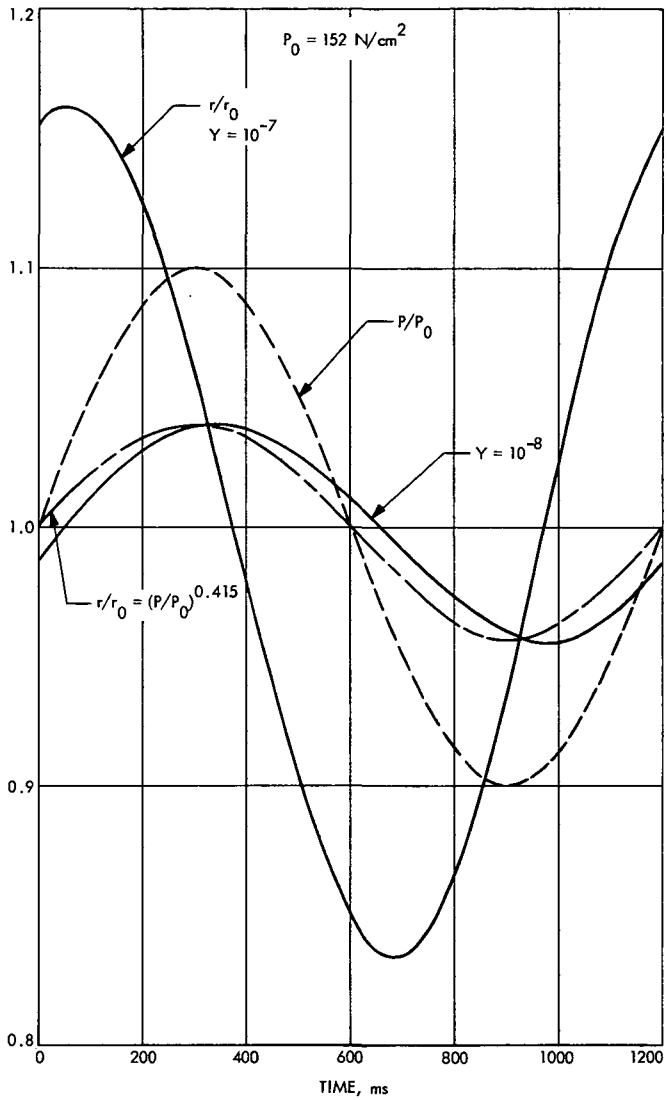

Fig. 34. Results of apparent transient burning rate calculations: sinusoidal pressure oscillation

Comparing the results with experimental $r'/\bar{r}$ data, Y values somewhere between 10^{-6} and 10^{-7} are needed for agreement, slightly larger than that indicated from the rapid depressurization calculations.

3. Conclusions. No attempts were made to measure the free electron concentration in the flame zone. A typical chemical analysis report for AP lots used in the test propellants showed alkali metal to be present in the form of $NaBrO_3$ and $NaClO_4$, 0.008% by weight each. Non-alkali metals accounted for 0.002% by weight. Spectrophotometer analysis of the pre-polymers used in the test propellants yielded the results shown in Table 3.

Table 3. Weight percent of sodium, potassium, and iron in propellant binder pre-polymers

Propellant	Pre-polymer	Percent by weight		
		Sodium	Potassium	Iron
540A	PPG	0.7×10^{-4}	0.3×10^{-4}	0.6×10^{-4}
HTPB	R-45	13×10^{-4}	0.3×10^{-4}	1.0×10^{-4}
CTPB	HC-434	49×10^{-4}	1.0×10^{-4}	7.0×10^{-4}
A-13 (T-burner driver propellant)	PBAN-787	13×10^{-4}	0.5×10^{-4}	34×10^{-4}

Due to the electron affinity of the halogen species present, equilibrium thermochemical calculations predict free electron mole fractions of less than 10^{-8}. However, as recently pointed out for solid-propellant rocket exhaust plume after-burning, electrical properties calculations based on the assumption that local thermochemical equilibrium is established can be greatly in error (Ref. 32).

We have tried to draw some overall conclusions based on the results of these calculations. It seems safe to conclude that the unrealistic regression rate measurements obtained in the T-burner and in the highest bomb depressurization rate experiments, discussed at the start of this section, can be accounted for by flame ionization effects on the microwave measurement. Considering the rapid depressurization experiments as a whole, it is concluded that for increasingly greater pressure gradients, the absolute values, but not the overall nature of the microwave regression measurements, are probably somewhat in error because of flame ionization effects. For example, throughout the pressure transient the experimental regression rate measurements generally fell below the steady-state rate at the corresponding pressure. The preceding calculations predict the real disparity between the two regression rates to be even greater, since for low free electron concentrations the apparent rate is supposedly greater than the actual value.

X. Summary and Conclusions

A microwave Doppler shift system was developed for the purpose of measuring the instantaneous regression rates of solid propellants during rapid pressure transients. Experiments were conducted to verify the spatial and time resolution of the system, the effect of propellant surface irregularities and compressibility on the measurements, and the accuracy of the system for quasi-steady-state regression rate measurements.

The microwave system was used in two different transient combustion experiments: in a rapid depressurization bomb and in the high-frequency acoustic pressure environment of a T-burner. PU, HTPB, and CTPB/AP composite propellants were tested. The results of the rapid depressurization experiments can be summarized as follows:

(1) There was a delay in the response of the regression rate to the initial depressurization, i.e., at $t = 0$, $dr/dt = 0$. For the PU binder propellant this delay diminished with increasing rate of depressurization. The longer delays for the PB binder propellants persisted up to the highest depressurization rates tested.

(2) Following this delay, the measured rate dropped abruptly, either continuing all the way to zero (and sometimes below), or recovering and eventually going to zero or the ambient pressure rate.

(3) During the pressure transient, the measured resultant regression rates (uncorrected for propellant compressibility effects) generally fell near or below the steady-state rate at the corresponding pressure.

(4) For the PU binder propellant, the measured regression rate exhibited rather irregular oscillations, not evident in the pressure signal, in tests near the critical depressurization rates for extinguishment. With increasing rate of depressurization the amplitude of the oscillations first increased and then diminished and eventually disappeared. The oscillations were roughly below 100 Hz in frequency, with the frequency decreasing with decreasing rate of depressurization.

(5) The HTPB and CTPB binder propellants were more difficult to extinguish, requiring twice as great initial depressurization rates in order to achieve extinction. The measured regression rates exhibited a characteristic single oscillation that disappeared with increasing rate of depressurization. For no-quenches the propellants were relatively slow in recovering to their predicted ambient pressure burning rates.

(6) As has been reported by others, the nature of the final portion of the pressure transient was found to be critical in determining whether or not extinguishment of combustion occurred.

The regression rate data seem to reinforce the description of rapid depressurization extinction presented by Steinz and Selzer (Ref. 10). Comparisons with the only other known transient data, that of Yin and Hermance (Refs. 21 and 28), yielded both points of agreement and disagreement.

Unreasonably high oscillatory regression rates, one to five or more times the measured mean rate, were obtained in the T-burner experiments. With frequencies in the 800–850 Hz range, the regression rate was found to lead the pressure by a phase angle of approximately 60 deg.

The T-burner results appeared to be more indicative of gaseous, rather than solid phase fluctuations. Therefore, using a modified version of the analytical procedure of Plett and Summerfield (Ref. 30), parametric calculations were performed on the effects of rapid variations in the flame zone ionization level on the apparent transient regression rate, as measured by the microwave Doppler shift technique. As found by Plett and Summerfield, the calculations predicted that to obtain accurate results the propellants must have a very low concentration of easily ionizable metals. For reasonable concentration levels, the predicted effects were of sufficient magnitude to account for the high response results of the T-burner experiments.

A direct comparison of the analytical predictions and experimental results yielded the conclusion that flame ionization effects probably produced some errors in the absolute values (erring on the high side), but not the general characteristics, of the regression rates measured in the rapid depressurization experiments. This disparity would be greatest for the highest rate-of-depressurization experiments. Since an accurate knowledge of the free electron concentrations in the propellant flame zones was not available, it is difficult to make a more quantitative statement as to the accuracy of the test measurements.

The present microwave system has demonstrated high spatial and time resolution, and, if propellants free of easily ionizable impurities can be prepared, should be applicable for combustion bomb transient regression rate measurements. Some type of *in situ* measurement of the electrical properties of the flame could possibly be used to make a correction for any residual ionization effects.

Finally, the propellant compressibility effects tests illustrated a possible additional application for the high spatial resolution of the test system, as a means of accurately determining the bulk modulus of solid propellants.

Appendix

Plasma Effects Analytical Model

The calculation of the phase change at the burning surface involves matching boundary conditions. Because the wave decays exponentially in the plasma region, the region can be assumed to extend indefinitely without loss of accuracy. In the propellant and transition regions there are waves in both the positive and negative x-directions. Since the plasma has been assumed to extend indefinitely, there is only a wave in the positive x-direction. The incident wave has the form $A \exp [i(\omega t - k_1 x)]$.

Since all of the waves have the $\exp(i\omega t)$ term, can it be disregarded. The arbitrary incident amplitude A will be allowed to assume the value of unity. The reflected wave in the propellant will then be $A_1 \exp [ik_1 x]$. In the transition region, the two waves will be $A_2 \exp [-ik_2 x]$ and $A_3 \exp [ik_2 x]$, and in the plasma, $A_4 \exp [-ik_3 x]$ (see Fig. A-1). The wave propagation exponents can be calculated since the properties of the different regions are known. This leaves the four amplitudes as the only unknowns. Matching boundary conditions provides two equations for each interface. The four equations solved simultaneously give values for the various amplitudes. Only A_1, however, is of any real interest. A_1 will in general be complex:

$$A_1 = |A_1| \exp [i\phi_s] \tag{A-1}$$

The phase change at the surface, ϕ_s, is the desired result.

The four boundary conditions are:

$$1 + A_1 = A_2 + A_3 \tag{A-2}$$

$$k_1(1 - A_1) = k_2(A_2 - A_3) \tag{A-3}$$

$$A_2 \exp [-ik_2 d] + A_3 \exp [ik_2 d] = A_4 \exp [-ik_3 d] \tag{A-4}$$

and

$$-k_2 A_2 \exp [-ik_2 d] + k_2 A_3 \exp [ik_2 d] = -k_3 A_3 \exp [-ik_3 d] \tag{A-5}$$

It now becomes necessary to calculate the wave propagation exponents. It is here that the properties of the waveguide become important. The wave exponents can be found by the expression:

$$k = \frac{2\pi}{\lambda_0} \sqrt{\epsilon - \left(\frac{\lambda_0}{\lambda_c}\right)^2} \tag{A-6}$$

where ϵ is the dielectric constant, λ_0 the free space wavelength of the microwave reference signal, and λ_c the cutoff wavelength in the empty waveguide. The dielectric constant of the propellant was taken to be 4.8. In the gaseous transition region, the dielectric constant is approximately unity. This gives a complex value for k_2, such that

$$k_2 = i\gamma \tag{A-7}$$

The dielectric constant in a plasma has both real and complex parts, and can be calculated if the electron concentration in the plasma is known. The complex dielectric constant of the plasma is $\epsilon' + i\epsilon''$. It is derived from

$$k_3 = \epsilon k_0 \tag{A-8}$$

and the expression for k_3 quoted by Plett and Summerfield. Thus, it is found that

$$(\epsilon')^2 = \frac{1}{2}\left[\left[1 - \frac{(\omega_p/\omega)^2}{1 + (\nu_c/\omega)^2}\right] + \left\{\left[1 - \frac{(\omega_p/\omega)^2}{1 + (\nu_c/\omega)^2}\right]^2 + \left[\frac{(\omega_p/\omega)^2}{1 + (\nu_c/\omega)^2}\right]^2 \left[\frac{\nu_c}{\omega}\right]^2\right\}^{1/2}\right] \tag{A-9}$$

$$(\epsilon'')^2 = (\epsilon')^2 - \left[1 - \frac{(\omega_p/\omega)^2}{1 + (\nu_c/\omega)^2}\right] \tag{A-10}$$

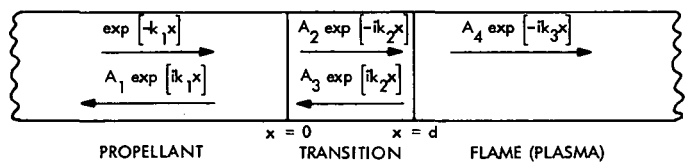

Fig. A-1. Wave model

Expressions for ν_c, the electron collision frequency, and ω_p, the plasma frequency, are obtained from Plett and Summerfield:

$$\nu_c = 1.21 \times 10^{11} P(\text{atm}) \tag{A-11}$$

$$\omega_p = 5.64 \times 10^4 (n_e)^{1/2} \tag{A-12}$$

The plasma density n_e, in electrons per cm^3, is

$$n_e = 2.687 \times 10^{19} P_e(\text{atm}) \tag{A-13}$$

The electron partial pressure, P_e, is given by the equation

$$P_e = \frac{-K_{ie} + (K_{ie}^2 + 4 K_{ie} PY)^{1/2}}{2} \tag{A-14}$$

where K_{ie} is the ionization equilibrium constant and Y the mole fraction of ionizable species. The ionization equilibrium constant in turn is obtained from the expression

$$K_{ie} = T^{2.5} \times 10^{-6.49-(23703E_0/4.573T)} \tag{A-15}$$

The ionization potential, E_0, was taken to be the value for sodium, 5.12 eV. A flame temperature, T, of 2800°K was assumed.

The only remaining unknowns are Y, d, and P, which are inputs for each calculation. As an approximation, during depressurization the gas in the transition zone is assumed to obey the perfect gas law, so that

$$d = d_0\left(\frac{P_0}{P}\right) \tag{A-16}$$

where d_0 is the initial value of d.

This is sufficient information to obtain results corresponding roughly to those obtained by Plett and Summerfield. Solving for ϕ_s,

$$\phi_s = \tan^{-1}\left[\frac{2k_1\gamma(1 - B^2(X^2 + z^2))}{k_1^2(1 + BX)^2 - \gamma^2B^2z^2 - \gamma^2(1 - BX)^2 + k_1^2B^2z^2}\right] \tag{A-17}$$

where

$$B = \frac{\exp(-2\gamma d)}{\alpha^2 + (\gamma + \beta)^2} \tag{A-18}$$

$$X = \gamma^2 - \alpha^2 - \beta^2 \tag{A-19}$$

and

$$z = -2\alpha\gamma \tag{A-20}$$

α and β are the real and imaginary parts of the complex wave propagation exponents in the plasma:

$$k_3 = \alpha + i\beta \tag{A-21}$$

Once ϕ_s is obtained, the calculation of the apparent regression rate becomes relatively straightforward. Rewriting Eq. (8) for the apparent burning rate as determined by the microwave Doppler phase shift technique,

$$r = \frac{\dot{\phi}\lambda_p}{720°} \tag{A-22}$$

where now

$$\dot{\phi} = \dot{\phi}_d + \dot{\phi}_s \tag{A-23}$$

and ϕ_d is the Doppler phase shift. Since it is r/r_0 which is ultimately desired, the value for r given in Eq. (A-22) is divided by r_0:

$$r_0 = \frac{\dot{\phi}_0\lambda_p}{720°} \tag{A-24}$$

However, since there is a constant pressure at $t = 0$, $\dot{\phi}_0 = \dot{\phi}_{d_0}$. Therefore,

$$\frac{r}{r_0} = \frac{\dot{\phi}_d}{\dot{\phi}_{d_0}} + \frac{\dot{\phi}_s}{\dot{\phi}_{d_0}} \tag{A-25}$$

In order to calculate $\dot{\phi}_{d_0}$, a value for r_0 must be assumed. For the purpose of this discussion r_0 was set equal to 0.5 cm/s at a P_0 value of 203 N/cm^2 (20 atm). λ_p must also be calculated. For a waveguide filled with dielectric ϵ, λ_p is given by

$$\lambda_p = \frac{2\pi}{k_1} = \frac{\lambda_0}{\sqrt{\epsilon - \left(\frac{\lambda_0}{\lambda_c}\right)^2}} \tag{A-26}$$

The cutoff wavelength λ_c for the primary mode of a circular waveguide is

$$\lambda_c = \frac{2\pi a}{1.841} \tag{A-27}$$

where a, the radius of the waveguide, has been taken to be 0.625 cm.

Having obtained λ_p, a value for $\dot{\phi}_{d_0}$ of 202°/s was obtained from Eq. (A-24).

The first term on the right side of Eq. (A-25) is the actual propellant regression rate as measured by the Doppler phase shift. Per Ref. 30, the actual transient regression rate is assumed to obey the rate law, $r = aP^n$. The pressure exponent was evaluated to correspond approximately to that for 540A propellant:

$$\frac{r}{r_0} = \left(\frac{P}{P_0}\right)^{0.415} \tag{A-28}$$

Incorporating this and the calculated value for $\dot{\phi}_{d_0}$, Eq. (A-25) becomes

$$\frac{r}{r_0} = \left(\frac{P}{P_0}\right)^{0.415} + \frac{\phi_s}{202°/s} \tag{A-29}$$

For the assumed transient pressure expression $\dot{\phi}_s$, the change of phase due to the change in the plasma density was evaluated as $\Delta\phi_s/\Delta t$ for discrete time steps corresponding to discrete pressure changes; from whence Eq. (A-29) provided values for r/r_0.

Nomenclature

A ratio of microwave test signal to reference signal amplitudes

$A_1,\cdots,A_4$ amplitude of various microwaves (see Fig. A-1)

a radius of circular waveguide; also pre-exponential term in burning rate law

B defined by Eq. (A-18)

b waveguide path length (see Fig. 2); also exponential constant term in Eq. (10)

c waveguide path length (see Fig. 2)

d width of transition zone

E_0 ionization potential of ionizable species (Na)

K_{ie} ionization equilibrium constant

k_p microwave propagation constant in propellant

k_w microwave propagation constant in empty rectangular waveguide

k_0 wave propagation exponent in free space

k_1 wave propagation exponent in propellant (Appendix)

k_2 wave propagation exponent in transition region

k_3 wave propagation exponent in flame (plasma)

ℓ propellant sample length

ℓ_0 total propellant length burned in a test

n pressure exponent in burning rate law

n_e plasma electron density

P pressure

P_e electron partial pressure

r apparent propellant regression rate

r' amplitude of regression rate oscillations

$\bar{r}$ mean regression rate

T flame temperature

t time

X defined by Eq. (A-19)

x dimension

Y mole fraction of ionizable species (Na)

z defined by Eq. (A-20)

α,β real and imaginary parts of k_3 (Eq. A-21)

γ complex value for k_2 (Eq. A-7)

ϵ dielectric constant

ϵ',ϵ'' real and imaginary parts of dielectric constant in plasma

λ_c cutoff wavelength in empty waveguide

λ_p wavelength of microwave in propellant

λ_0 wavelength of microwave reference signal in free space

ν_c collision frequency of electrons with neutrals

ϕ phase difference between microwave test and reference signals

ϕ_d Doppler phase shift component of ϕ

ϕ_s burning surface phase shift component of ϕ

ϕ_0 total microwave phase shift in a test

ω angular frequency of microwave signal

ω_i angular frequency of incident microwave signal

ω_p plasma frequency

ω_r angular frequency of microwave signal reflected from regressing propellant surface

$\Delta\omega$ beat frequency of superimposed microwave signals

Superscript

$\cdot$ rate of change with time

Subscript

0 steady-state value prior to pressure transient ($t < 0$)

References

1. von Elbe, G., "Theory of Solid Propellant Ignition and Response to Pressure Transients" (Paper Unclassified), *Bulletin of the 19th Interagency Solid Propulsion Meeting,* CPIA Publication No. 18, Vol. III, pp. 95–127, Silver Spring, Md., July 1963 (Confidential).

2. Cohen, N. S., Paul, B. E., and Fong, L. Y., "Solid Propellant Burning Rate Under Transient Heating and Extinguishment via L* Instability," *Bulletin of the 1st ICRPG Combustion Conference,* CPIA Publication No. 68, pp. 491–506, Silver Spring, Md., Jan. 1965.

3. Parker, K. H., and Summerfield, M., "Response of the Burning Rate of a Solid Propellant to a Pressure Transient," AIAA Paper No. 66-683, presented at the Second Propulsion Joint Specialists Conference, Colorado Springs, Colo., June 1966.

4. Horton, M. D., Bruno, P. S., and Graesser, E. C., "Depressurization Induced Extinction of Burning Solid Propellant," *AIAA J.*, Vol. 6, No. 2, pp. 292–297, Feb. 1968.

5. Culick, F. E. C., "A Review of Calculations for Unsteady Burning of a Solid Propellant, *AIAA J.*, Vol. 6, No. 12, pp. 2241–2255, Dec. 1968.

6. Merkle, C. L., Turk, S. L., and Summerfield, M., "Extinguishment of Solid Propellants by Depressurization: Effects of Propellant Parameters," AIAA Paper No. 69-176, presented at the AIAA 7th Aerospace Sciences Meeting, New York, N. Y., Jan. 1969.

7. Wooldridge, C. E., and Marxman, G. A., "Nonlinear Solid Propellant Burning Rate Behavior During Abrupt Pressure Excursions," AIAA Paper No. 69-172, presented at the AIAA 7th Aerospace Sciences Meeting, New York, N. Y., Jan. 1969.

8. Hiroki, T., and Fletcher, E. A., "Theoretical Study of Propellant Behavior During Thrust Chamber Depressurization," *AIAA J.*, Vol. 7, No. 10, pp. 1884–1890, Oct. 1969.

9. Summerfield, M., et al., "Theory of Dynamic Extinguishment of Solid Propellants With Special Reference to Nonsteady Heat Feedback Law," AIAA Paper No. 7-667, presented at the AIAA 6th Propulsion Joint Specialist Conference, San Diego, Calif., June 1970.

10. Steinz, J. A., and Selzer, H., "Depressurization Extinguishment of Composite Solid Propellants: Flame Structure, Surface Characteristics, and Restart Capability," *Combustion Science and Technology,* Vol. 3, pp. 25–36, 1971.

11. Fletcher, E. H., and Bunde, G. W., "An Experimental Investigation of Gas Evolution from a Solid Rocket Propellant During Pressure Transients," AIAA Paper No. 65-104, presented at the AIAA 2nd Aerospace Sciences Meeting, New York, N. Y., Jan. 1965.

12. Barrere, M., "Transient Response of Solid Propellant Combustion," *Astronaut. Acta,* Vol. 15, Nos. 5 and 6, pp. 633–640, 1970.

13. Fletcher, E. A., and Hiroki, T., "Gas Evolution from Solid Propellants During Pressure Decays," *AIAA J.*, Vol. 4, No. 12, pp. 2222–2224, Dec. 1966.

References (contd)

14. Ciepluch, C., "Effect of Rapid Pressure Decay on Solid Propellant Combustion," *ARS J.*, Vol. 31, No. 11, pp. 1584–1586, 1961.

15. Baer, H. D., Ryan, N. W., and Schulz, E. B., "Spectra and Temperature of Propellant Flames During Depressurization," *AIAA J.*, Vol. 9, No. 5, pp. 869–875, May 1971.

16. Marshakov, V. N., and Leipunskii, O. I., "Propellant-Burning Mechanism in the Presence of a Pressure Drop," *Combustion, Explosion and Shock Waves*, Vol. 5, No. 1, pp. 1–3, 1969.

17. Jenson, G. C., *A Stop-Start Study of Solid Propellants*, Final Technical Report, NASA CR-66488, UTC 2243-FR. United Technology Center, Sunnyvale, Calif., Nov. 1967.

18. Price, E. W., "Experimental Solid Rocket Combustion Instability," *Tenth Symposium (International) on Combustion Proceedings*, The Combustion Institute, pp. 1067–1080, 1965.

19. Krier, H., Mathes, H. B., Price, E. W., and Summerfield, M., "Entropy Waves Produced in Oscillatory Combustion of Solid Propellants," AIAA Paper No. 68-499, presented at the ICRPG/AIAA 3rd Solid Propulsion Conference, Atlantic City, N. J., June 1968.

20. Eisel, J. L., Ryan, N. W., and Baer, A. D., "Flame Spectra of Solid Propellants During Unstable Combustion," AIAA Paper No. 72-32, presented at the AIAA 10th Aerospace Sciences Meeting, San Diego, Calif., Jan. 1972.

21. Yin, C. F., and Hermance, C. E., "Continuous Measurement of Transient Burning Rates of a Composite Propellant Undergoing Rapid Depressurization," AIAA Paper No. 71-173, presented at the AIAA 9th Aerospace Sciences Meeting, New York, N. Y., Jan. 1971.

22. Cole, R. B., *High Pressure Solid Propellant Combustion Studies Using a Closed Bomb*, Report S-68. Rohm and Haas Company, Redstone Arsenal Research Division, Huntsville, Ala., Aug. 1965.

23. Green, D. T., *Application of Microwaves to the Measurement of Solid Propellant Burning Rates and to Non-Destructive Testing*, Technical Memorandum 514. Rocket Propulsion Establishment, Westcott, United Kingdom, Mar. 1968.

24. Wood, H. L., *A Study of the Application of Microwave Techniques to the Measurement of Solid Propellant Burning Rates*, Final Report on NASA Grant NGR 47-004-024. Virginia Polytechnic Institute, Blacksburg, Va., May 1970.

25. Shelton, S. V., "A Technique for Measurement of Solid Propellant Burning Rates During Rapid Pressure Transients," *Bulletin of the 4th ICRPG Combustion Conference*, CPIA Publication No. 162, Vol. I, pp. 361–372, Silver Spring, Md., Dec. 1967.

26. Perry, E. H., *Investigation of the T-burner and its Role in Combustion Instability Studies*, PhD thesis. Daniel & Florence Guggenheim Jet Propulsion Center, California Institute of Technology, Pasadena, Calif., 1970.

References (contd)

27. Strand, L. D., *Summary of a Study of the Low-Pressure Combustion of Solid Propellants,* Technical Report 32-1242. Jet Propulsion Laboratory, Pasadena, Calif., Apr. 15, 1968.

28. Yin, C. F., and Hermance, C. E., *Continuous Measurement of the Burning Rate of a JANNAF Standard Propellant,* University of Waterloo, Ontario, Canada.

29. Jensen, G. E., *An Experimental Study of Solid Propellant Extinguishment by Rapid Depressurization,* Final Technical Report, NASA CR-66747, UTC 2311-FR. United Technology Center, Sunnyvale, Calif., Mar. 1969.

30. Plett, E. G., and Summerfield, M., *Remarks on the Use of Microwaves for Measurement of Solid Propellant Burning Rates During Pressure Transients,* Preliminary Draft for Discussion, Princeton University, Princeton, N. J., Sept. 15, 1970.

31. Culick, F. E. C., and Dehority, G. L., "An Elementary Calculation for the Burning Rate of Composite Solid Propellants," *Combustion Science and Technology,* Vol. 1, pp. 193–204, 1969.

32. Jensen, D. E., and Pergament, H. S., "Effects of Nonequilibrium Chemistry on Electrical Properties of Solid Propellant Exhaust Plumes," *Combustion and Flame,* Vol. 17, pp. 115–124, 1971.